Article type: Research

Whole genome comparisons of ergot fungi reveals the divergence and evolution of species within the genus *Claviceps* are the result of varying mechanisms driving genome evolution and host range expansion

Stephen A. Wyka[1], Stephen J. Mondo[1,2], Miao Liu[3], Jeremy Dettman[3], Vamsi Nalam[1], Kirk D. Broders[4*]

[1] Department of Agricultural Biology, Colorado State University, Fort Collins, CO 80523, USA.

[2] U.S. Department of Energy Joint Genome Institute, Berkeley, CA 94720, USA.

[3] Ottawa Research and Development Centre, Agriculture and Agri-Food Canada, Ottawa K1A 0C6, Canada.

[4] Smithsonian Tropical Research Institute, Apartado 0843-03092 Panamá, República de Panamá.

[*] Corresponding authors: Kirk D. Broders, email: BrodersK@si.edu

Abstract:

The genus *Claviceps* has been known for centuries as an economically important fungal genera for pharmacology and agricultural research. Only recently have researchers begun to unravel the evolutionary history of the genus, with origins in South America and classification of four distinct sections through ecological, morphological, and metabolic features (*Claviceps* sects. *Citrinae, Paspalorum*, *Pusillae*, and *Claviceps*). The first three sections are additionally characterized by narrow host range, while sect. *Claviceps* is considered evolutionarily more successful and adaptable as it has the largest host range and biogeographical distribution. However, the reasons for this success and adaptability remain unclear. Our study elucidates factors influencing adaptability by sequencing and annotating 50 *Claviceps* genomes, representing 21 species, for a comprehensive comparison of genome architecture and plasticity in relation to host range potential. Our results show the trajectory from specialized one-speed genomes (sects. *Citrinae* and *Paspalorum*) towards adaptive two-speed genomes (sects. *Pusillae* and *Claviceps*) through co-localization of transposable elements around predicted effectors and a putative loss of repeat-induced point mutation resulting in unconstrained tandem gene duplication coinciding with increased host range potential and speciation. Alterations of genomic architecture and plasticity can substantially influence and shape the evolutionary trajectory of fungal pathogens and their adaptability. Furthermore, our study provides a large increase in available genomic resources to propel future studies of *Claviceps* in pharmacology and agricultural research, as well as, research into deeper understanding of the evolution of adaptable plant pathogens.

Keywords: adaptive evolution, gene family expansion, two-speed genomes, fungal plant pathogens, RIP, ergot

Introduction:

Fungi, particularly phytopathogenic species, are increasingly being utilized to gain insight into the evolution of eukaryotic organisms, due to their adaptive nature and unique genome structures (Gladieux *et al.* 2014; Dong *et al.* 2015). Adaptation and diversification of fungal species can be mediated by changes in genome architecture and plasticity such as genome size, transposable element (TE) content, localization of TEs to specific genes, genome compartmentalization, gene duplication rates, recombination rates, and presence/absence polymorphism of virulence factors (Dong *et al.* 2015; Möller & Stukenbrock 2017). The presence or absence of repeat-induced point (RIP) mutation is also an important mechanism for fungal genome evolution, as RIP works on a genome-wide scale to silence transposable elements and duplicated genes, which can also "leak" onto neighboring genes (Galagan *et al.* 2003, 2004; Raffaele & Kamoun 2012; Urguhart *et al.* 2018; Möller & Stukenbrock 2019). It is becoming increasingly evident that variations in these factors can be used to classify genomes as a one-speed (one-compartment), such as the powdery mildew fungi *Blumeria graminis* f.sp. *hordei* and f.sp *tritici*, two-speed (two-compartment), such as the late blight pathogen *Phytophthora infestans*, or multi-speed (multi-compartment) such as the multi-host pathogen *Fusarium oxysporum* (Dong *et al.* 2015; Frantzeskakis *et al.* 2019). These different "speeds" are characterized by their potential adaptability such that one-speed genomes are often considered less-adaptable, while two-speed and multi-speed genomes are often considered more-adaptable (Dong *et al.* 2015; Frantzeskakis *et al.* 2019; Möller & Stukenbrock 2019).

61 The ergot fungi of the genus *Claviceps* (Ascomycota, Hypocreales) are biotrophic species
62 that share a specialized ovarian-specific non-systemic parasitic lifestyle with their grass hosts
63 (Píchová *et al.* 2018). Infections are fully restricted to individual unpollinated ovaries (Tudzynski
64 and Scheffer 2004), and the fungus actively manages to maintain host cell viability to obtain
65 nutrients from living tissue through a complex cross-talk of genes related to pathogenesis, such
66 as secreted effectors, secondary metabolites, or cytokinin production (Hinsch *et al.* 2015, 2016;
67 Oeser *et al.* 2017; Kind *et al.* 2018a, 2018b). Species of *Claviceps* are most notably known for
68 their production of toxic alkaloids and secondary metabolites but are also known for their
69 expansive host range and negative impact on global cereal crop production and livestock
70 farming. These negative effects on human and livestock health are the primary reason *Claviceps*
71 species are referred to as plant pathogens. However, under the light of co-evolution with their
72 grass hosts some *Claviceps* species are considered conditional defensive mutualists with their
73 hosts as they prevent herbivory and can improve host fitness (Raybould *et al.* 1998; Fisher *et al.*
74 2007; Wäli *et al.* 2013).
75 The genus *Claviceps* contains 59 species divided into four sections; sects. *Claviceps*,
76 *Pusillae*, *Citrinae*, and *Paspalorum* (Píchová *et al.* 2018). It was postulated that sects. *Citrinae*
77 and *Paspalorum* originated in South America, while sect. *Pusillae* experienced speciation
78 throughout the Eocene, Oligocene, and Miocene as these species encountered newly emergent
79 PACMAD warm-season grasses (subfamilies Panicoideae, Aristidoideae, Chloridoideae,
80 Micrairoideae, Arundinoideae, Danthonioideae) when an ancestral strain was transferred from
81 South America to Africa (Píchová *et al.* 2018). In contrast, the crown node of sect. *Claviceps* is
82 estimated at 20.4 Mya and was followed by a radiation of the section corresponding to a host
83 jump from ancestral sedges (Cyperaceae) to the BOP clade (cool-season grasses; subfamilies

84 Bambusoideae, Oryzoideae (syn: Ehrhartoideae) (Soreng *et al.* 2015), Pooideae) in North
85 America (Bouchenak-Khelladi *et al.* 2010; Píchová *et al.* 2018). Section *Claviceps* has the
86 largest host range with *C. purpurea sensu stricto* (s.s.) having been reported on up to 400
87 different species in clade BOP (Alderman *et al.* 2004, Píchová *et al.* 2018) across six tribes, and
88 retains the ability to infect sedges (Cyperaceae) (Jungehülsing and Tudzynski 1997). In contrast,
89 sect. *Pusillae* is specialized to the tribes Paniceae and Andropogoneae, and sects. *Citrinae* and
90 *Paspalorum* only infect members of tribe Paspaleae and tribe Cynodonteae, respectively
91 (Píchová *et al.* 2018). The shared specialized infection life cycle of the *Claviceps* genus, the
92 drastic differences in host range potential of different species, and geographic distribution
93 represent a unique system to study the evolution and host adaptation of eukaryotic organisms.
94 Despite their ecological and agriculture importance, little is known about the evolution
95 and genomic architecture of these important fungal species in comparison to other cereal
96 pathogens such as species in the genera *Puccinia* (Cantu *et al.* 2013; Kiran *et al.* 2016, 2017),
97 *Zymoseptoria* (Grandaubert *et al.* 2015, 2019; Estep *et al.* 2015; Poppe *et al.* 2015; Testa *et al.*
98 2015; Wu *et al.* 2017; Stukenbrock & Dutheil 2018), or *Fusarium* (Kvas *et al.* 2009; Ma *et al.*
99 2010; Rep & Kistler 2010; Watanabe *et al.* 2011; Sperschneider *et al.* 2015). Unfortunately, the
100 lack of genome data for the *Claviceps* genus has hampered our ability to complete comparative
101 analyses to identify factors that are influencing the adaptation of *Claviceps* species across the
102 four sections in the genus, and the mechanisms by which species of sect. *Claviceps* have adapted
103 to such a broad host range, in comparison to the other three sections. Here we present the
104 sequences and annotations of 50 *Claviceps* genomes, representing 19 species, for a
105 comprehensive comparison of the genus to understand evolution within the genus *Claviceps* by
106 characterizing the genomic plasticity and architecture in relation to adaptive host potential. Our

107 analysis reveals the trajectory from specialized one-speed genomes (sects. *Citrinae* and
108 *Paspalorum*) towards adaptive two-speed genomes (sects. *Pusillae* and *Claviceps*) through co-
109 localization of transposable elements around predicted effectors and a putative loss of RIP
110 resulting in tandem gene duplication coinciding with increased host range potential.
111
112 **Materials and Methods:**
113 *Sample acquisition*:
114 Field collected samples (Clav) were surfaced sterilized, allowed to grow as mycelia, and
115 individual conidia transferred to make single spore cultures. Thirteen cultures were provided by
116 Dr. Miroslav Kolařík from the Culture Collection of Clavicipitaceae (CCC) at Institute of
117 Microbiology, Academy of Sciences of the Czech Republic. Raw Illumina reads for samples
118 (LM28, LM582, LM78, LM81, LM458, LM218, LM454, LM576, and LM583) were
119 downloaded from NCBI's SRA database. Raw Illumina reads from an additional 21 LM samples
120 were generated by Dr. Liu's lab (AAFC), sequencing protocol of these 21 samples followed
121 Wingfield *et al.* (2018). Summarized information can be found in Additional file 1: Table S1.
122
123 *Preparation of genomic DNA*:
124 Cultures grown on cellophane PDA plates were used for genomic DNA extraction from
125 lyophilized mycelium following a modified CTAB method (Doyle and Doyle 1987; Wingfield *et*
126 *al.* 2018) without using the RNase Cocktail™ Enzyme Mix, only RNASE A was used. DNA
127 contamination was checked by running samples on a 1% agarose gel and a NanoDrop One[c]
128 (Thermo Fishcer Scientific). Twenty samples (7 Clav and 13 CCC) were sent to BGI-Hong Kong
129 HGS Lab for 150-bp paired-end Illumina sequencing on a HiSeq™ 4000.

130

131 *Genome assembly:*

132 Preliminary data showed that raw reads of LM458 were contaminated with bacterial
133 DNA but showed strong species similarity to Clav32 and Clav50. To filter out the bacterial DNA
134 sequences, reads of LM458 were mapped against the assembled Clav32 and Clav50 genomes
135 using BBSplit v38.41 (Bushnell 2014). All forward and reverse reads mapped to each of the
136 genomes were concatenated, respectively. Both sets were then interleaved to remove duplicates
137 and used for further analysis. Reads for all 50 samples were checked for quality with FastQC
138 v0.11.5 (Andrews 2010) and trimmed with Trimmomatic v0.36 (Bolger *et al.* 2014) using the
139 commands (SLIDINGWINDOW:4:20 MINLEN:36 HEADCROP:10) to remove poor quality
140 data, only paired end reads were used. To better standardize the comparative analysis all 50
141 sample were subject to *de novo* genome assembly with Shovill v0.9.0
142 (https://github.com/tseemann/shovill) using SPAdes v3.11.1 (Nurk *et al.* 2013) with a minimum
143 contig length of 1000 bp.

144 The reference genomes of *C. purpurea* strain 20.1 (SAMEA2272775), *C. fusiformis* PRL
145 1980 (SAMN02981339), and *C. paspali* RRC 1481 (SAMN02981342) were downloaded from
146 NCBI. Proteins for *C. fusiformis* and *C. paspali* were not available on NCBI so they were
147 extracted from GFF3 files provided by Dr. Chris Schardl and Dr. Neil Moore, University of
148 Kentucky, corresponding to the 2013 annotations (Schardl *et al.* 2013) available at
149 http://www.endophyte.uky.edu. Reference genomes were standardized for comparative analysis
150 with our 50 annotated genomes, by implementing a protein length cutoff of 50 aa and removal of
151 alternatively spliced proteins in *C. fusiformis* and *C. paspali*, only the longest spliced protein for
152 each locus remained.

153

154 *Transposable elements:*

155 Transposable elements (TE) fragments were identified following procedures for
156 establishment of *de novo* comprehensive repeat libraries set forth in Berriman *et al.* (2018)
157 through a combined use of RepeatModeler v1.0.8 (Smit & Hubley 2015), TransposonPSI (Hass
158 2010), LTR_finder v1.07 (Xu & Wang 2007), LTR_harvest v1.5.10 (Ellinghaus *et al.* 2008),
159 LTR_digest v1.5.10 (Steinbiss *et al.* 2009), Usearch v11.0.667 (Edgar 2010), and
160 RepeatClassifier v1.0.8 (Smit & Hubley 2015) with the addition of all curated fungal TEs from
161 RepBase (Bao *et al.* 2015). RepeatMasker v4.0.7 (Smit *et al.* 2015) was then used to soft mask
162 the genomes and identify TE regions. TE content was represented as the proportion of the
163 genome masked by TE regions determined by RepeatMasker, excluding simple and low
164 complexity repeats. These steps were automated through construction of a custom script,
165 TransposableELMT (https://github.com/PlantDr430/TransposableELMT).

166 Divergence landscapes for TEs in all 53 *Claviceps* genomes were generated using a
167 custom script
168 (https://github.com/PlantDr430/CSU_scripts/blob/master/TE_divergence_landscape.py) and the
169 RepeatMasker output results. The RepeatMasker results were also used with the respective GFF3
170 file from each genome to calculate the average distance (kbp) of each gene to the closest TE
171 fragment on the 5' and 3' flanking side. Values were calculated for predicted effectors, non-
172 effector secreted genes, non-secreted metabolite genes, and all other genes using a custom script
173 (https://github.com/PlantDr430/CSU_scripts/blob/master/TE_closeness.py).

174

175 *Genome annotation:*

176 AUGUSTUS v3.2.2 (Mario *et al.* 2008) was used to create pre-trained parameters files
177 using the reference *C. purpurea* strain 20.1, available EST data from NCBI, and wild-type
178 RNAseq data (SRR4428945) created in Oeser *et al.* (2017). RNA-seq data was subject to quality
179 check and trimming as above. All three datasets were also used to train parameter files for the *ab*
180 *initio* gene model prediction software's GeneID v1.4.4 (Blanco *et al.* 2007) and CodingQuarry
181 v2.0 (Testa *et al.* 2015). GeneID training followed protocols available at
182 http://genome.crg.es/software/geneid/training.html. For CodingQuarry training, RNA transcripts
183 were created *de novo* using Trinity v2.8.4 (Grabherr *et al.* 2011) on default settings and EST
184 coordinates were found by mapping the EST data to the reference genome using Minimap2 v2.1
185 (Li 2018).
186 Gene models for the 50 genomes were then predicted with GeneID and CodingQuarry
187 using the trained *C. purpruea* parameter files. CodingQuarry prediction was also supplemented
188 with transcript evidence by mapping the available EST and RNA-seq *C. purpurea* data to each
189 genome using Minimap2. BUSCO v3 (Waterhouse *et al.* 2018) was run on all 50 genomes using
190 the AUGUSTUS *C. purpurea* pre-trained parameter files as the reference organism and the
191 Sordariomyceta database. The resulting predicted proteins for each sample were used as training
192 models for *ab initio* gene prediction using SNAP (Korf 2004) and GlimmerHMM v3.0.1
193 (Majoros *et al.* 2004). Lastly, GeMoMa v1.5.3 (Keilwagen *et al.* 2016) was used for *ab initio*
194 gene prediction using the soft-masked genomes and the *C. purpruea* 20.1 reference files.
195 Funannotate v1.6.0 (Palmer & Stajich 2019) was then used as the primary software for
196 genome annotation. Funannotate additionally uses AUGUSTUS and GeneMark-ES (Ter-
197 Hovhannisyan *et al.* 2008) for *ab initio* gene model prediction, Exonerate for transcript and
198 protein evidence alignment, and EVidenceModeler (Hass *et al.* 2008) for a final weighted

199 consensus. All *C. purpurea* EST and RNAseq data were used as transcript evidence and the
200 Uniport Swiss-Prot database and proteins from several closely related species (*C. purpurea* strain
201 20.1, *C. fusiformis* PRL1980, *C. paspali* RRC1481, *Fusarium oxysporum f.sp. lycopersici* 4287,
202 *Pochonia chlamydosporia* 170, *Ustilago maydis* 521, and *Epichloe festucae* F1) were used as
203 protein evidence. The AUGUSTUS pre-trained *C. purpurea* files were used as BUSCO seed
204 species along with the Sordariomyceta database and all five *ab initio* predictions were passed
205 through the --other_gff flag with weights of 1. The following flags were also used in Funannotate
206 "predict": --repeats2evm, --optimize_augustus, --soft_mask 1000, --min_protlen 50. BUSCO
207 was used to evaluate annotation completeness using the Dikarya and Sordariomyceta databases
208 (odb9) with --prot on default settings.
209
210 *Functional annotation:*
211 Functional analysis was performed using Funannotate "annotate". The following analyses
212 were also performed on the three reference *Claviceps* genomes. Secondary metabolite clusters
213 were predicted using antiSMASH v5 (Blin *et al.* 2019) with all features turned on. Functional
214 domain annotations were conducted using eggNOG-mapper v5 (Huerta-Cepas *et al.* 2016, 2019)
215 on default settings and InterProScan v5 (Jones *et al.* 2014) with the --goterms flag. Phobius
216 v1.01 (Käll 2007) was used to assist in prediction of secreted proteins. In addition to these
217 analyses Funannotate also performed domain annotations through an HMMer search against the
218 Pfam-A database and dbCAN CAZYmes database, a BLASTp search against the MEROPS
219 protease database, and secreted protein predictions with SignalP v4.1 (Nielsen 2017).
220 For downstream analysis, proteins were classified as secreted proteins if they had signal
221 peptides detected by both Phobius and SignalP and did not possess a transmembrane domain as

222 predicted by Phobius and an additional analysis of TMHMM v2.0 (Krogh *et al.* 2001). Effector
223 proteins were identified by using EffectorP v2.0 (Sperschneider *et al.* 2018), with default
224 settings, on the set of secreted proteins for each genome. Transmembrane proteins were
225 identified if both Phobius and TMHMM detected transmembrane domains. Secondary metabolite
226 proteins were identified if they resided within metabolite clusters predicted by antiSMASH.
227 Proteins were classified as having conserved protein domains if they contained any Pfam or IPR
228 domains.
229
230 *Gene family identification and classification*:
231 OrthoFinder v2.3.3 (Emms & Kelly 2019) was run on default settings using Diamond
232 v0.9.25.126 (Buchfunk *et al.* 2015) to infer groups of orthologous gene clusters (orthogroups)
233 based on protein homology and MCL clustering. To more accurately place closely related genes
234 into clusters an additional 78 fungal genomes (Additional file 1 Table S3) with emphasis on
235 plant associated fungi of the order Hypocreales were added. To standardize, all 78 additional
236 genomes were subject to a protein length cutoff of 50 amino acids and genomes downloaded
237 from http://www.endophyte.uky.edu had alternatively spliced proteins removed. For downstream
238 analysis, orthogroups pertaining to the 53 *Claviceps* genomes were classified as secreted,
239 predicted effectors, transmembrane, metabolite, and conserved domain orthogroups if ≥50% of
240 the *Claviceps* strains present in a given cluster had at least one protein classified as such.
241
242 *Phylogeny and genome fluidity*:
243 Phylogenetic relationship of all 53 *Claviceps* genomes, with *Fusarium graminearum*, *F.*
244 *verticillioides*, *Epichloe festucae*, and *E. typhina* as outgroups, was derived from 2,002 single-

245 copy orthologs obtained from our OrthoFinder defined gene clusters (described above). This
246 resulted in a dataset of 114,114 amino acids sequences which were concatenated to create a
247 super-matrix and aligned using MAFFT v7.429 (Katoh & Standely 2013) on default settings.
248 Uninformative sites were removed using Gblocks v0.91 (Castresana 2000) on default settings.
249 Due to the large scale of the alignment maximum likelihood reconstruction was performed using
250 FastTree v2.1.11 (Price *et al.* 2010) using the WAG model of amino acid substitution with the -
251 gamma, -spr 4, -mlacc 2, -slownni, and -slow flag with 1000 bootstraps. MEGA X (Sudhir *et al.*
252 2018) was used for neighbor-joining (NJ) reconstruction using the JTT model of amino acid
253 substitution with gamma distribution and maximum parsimony (MP) reconstruction using the
254 tree bisection reconstruction (TBR) algorithm with 100 repeated searches. Nodal support for
255 both NJ and MP reconstructions were assessed with 1000 bootstraps. In addition, an alignment
256 and ML reconstruction was performed on each of the 2,002 protein sequences following the
257 procedure as above (MAFFT, Gblocks, FastTree). A density consensus phylogeny was created
258 from all gene trees using the program DensiTree v2.2.5 (Bouckaert & Heled 2014). PhyBin v0.3-
259 1 (Newton & Newton 2013) was used to cluster trees from three datasets (1: *Claviceps* genus
260 without outgroups, 2: sect. *Pusillae* species, 3: sect. *Claviceps* species) together to identify
261 frequencies of concordant topologies using the --complete flag with --editdist=2. To reduce
262 noise, from abundant incomplete lineage sorting in sect. *Claviceps*, we implemented a --
263 minbranchlen=0.015 for our *Claviceps* genus dataset.
264 Following methodologies established in Kislyuk *et al.* (2011) genomic fluidity, which
265 estimates the dissimilarity between genomes by using ratios of the number of unique gene
266 clusters to the total number of gene clusters in pairs of genomes averaged over randomly chosen
267 genome pairs from within a group on *N* genomes, was used to assess gene cluster dissimilarity

268 within the *Claviceps* genus. For a more detailed description refer to Kislyuk *et al.* (2011).
269 Datasets containing gene clusters from representative members of sect. *Pusillae*, sect. *Claviceps*,
270 *Clavieps* genus, and all *C. purpurea* strains were extracted from our OrthoFinder defined gene
271 clusters. Additional species- and genus-wide gene cluster datasets from the additional 78 fungal
272 genomes were extracted for comparative purposes. All section- and genus-wide datasets
273 contained one representative isolate from each species to reduce phylogenetic bias. Each
274 extracted dataset was used to calculate the genomic fluidity using a custom script
275 (https://github.com/PlantDr430/CSU_scripts/blob/master/pangenome_fluidity.py). The result
276 files for each dataset were then used for figure creation and two-sample two-sided z-test statistics
277 (Kislyuk *et al.* 2011) using a custom script
278 (https://github.com/PlantDr430/CSU_scripts/blob/master/combine_fluidity.py).
279
280 *Gene compartmentalization:*
281 A custom script
282 (https://github.com/PlantDr430/CSU_scripts/blob/master/genome_speed_hexbins.py) was used
283 to calculate local gene density measured as 5' and 3' flanking distances between neighboring
284 genes (intergenic regions). To statistically determine whether specific gene types had longer
285 intergenic flanking regions than all other genes within the genome we randomly sampled 100
286 each group of genes (specific gene vs. other genes) 1,000 times for both the 5' and 3' flanking
287 distances. Mann-Whitney U test was used to test for significance on all 2,000 subsets corrected
288 with Benjamini-Hochberg. Corrected p-values were averaged per flanking side and then together
289 to get a final p-value. Genes that appeared on a contig alone were excluded from analysis. For
290 graphical representation, genes that were located at the start of each contig (5' end) were plotted

291 along the x-axis, while genes located at the end of each contig (3' end) were plotted along the y-
292 axis.
293
294 *RIP and BLAST analyses*:
295 For all 53 genomes a self BLASTp v2.9.0+ search was conducted to identify best hit
296 orthologs within each genome with a cutoff e-value of 10^{-5} and removal of self-hits. This process
297 was automated, using a custom script
298 (https://github.com/PlantDr430/CSU_scripts/blob/master/RIP_blast_analysis.py). We further
299 examined if gene pairs with a pairwise identity of ≥80% were located next to each other and/or
300 separated by five or fewer genes. Fifty-six important *Claviceps* genes (Additional file 2: Table
301 S7) including the *rid-1* homolog (Freitag *et al.* 2002) were used in a BLASTp analysis to identify
302 the number of genes present that passed an e-value cutoff of 10^{-5}, 50% coverage, and 35%
303 identity. Genes that appeared as best hits for multiple query genes were only recorded once for
304 their overall best match. In addition, the web-based tool The RIPper (Van Wyk *et al.* 2019) was
305 used on default settings (1 kb windows in 500 bp increments) to scan whole-genomes for
306 presence of RIP and large RIP affected regions (LRARs).
307
308 *Statistical programs and plotting:*
309 Statistics and figures were generated using Python3 modules SciPy v1.3.1, statsmodel
310 v0.11.0, and Matplotlib v3.1.1. Heatmaps were generated using ComplexHeatmap v2.2.0 in R
311 (Gu 2016).
312
313 **Results:**

314 *Genome Assembly and Annotation*:

315 To provide a comprehensive view of variability across *Claviceps*, we sequenced and
316 annotated 50 genomes (19 *Claviceps* spp.), including *C. citrina* the single species of sect.
317 *Citrinae*, six species belonging to sect. *Pusillae*, and 44 genomes (12 species) belonging to sect.
318 *Claviceps*, of which 23 genomes belong to *C. purpurea* s.s. (Table 1; Additional file 1: Table
319 S1). The assemblies and annotations were of comparable quality to the reference strains (Table
320 1). A more detailed representation of the assembly and annotation statistics can be seen in Table
321 1 and Additional file 1: Figure S1, Table S2.

322 Overall, species of sect. *Claviceps* had better assemblies and annotations than species of
323 other sections regarding contig numbers, N50's, and BUSCO completeness scores (Table 1).
324 Nearly all species of sect. *Claviceps* showed higher BUSCO scores than the references, while
325 species of sects. *Pusillae* and *Citrinae* generally showed lower scores, likely due to their higher
326 TE content (average 34.9% ± 11.0%; Table 1). Exceptions to the low BUSCO scores were *C.*
327 *digitariae* and *C. maximensis* (sect. *Pusillae*), which had lower TE content, 20.0% and 19.8%,
328 respectively, than the rest of the species in sect. *Pusillae* (Table 1).

329

330 *Phylogenomics and genome fluidity:*

331 Orthologous gene clusters (orthogroups), which contain orthologs and paralogs, were
332 inferred from protein homology and MCL clustering using OrthoFinder. Across the 53 *Claviceps*
333 isolates and outgroups species *Fusarium graminearum*, *F. verticillioides*, *Epichloe festucae*, and
334 *E. typhina*. We identified 2,002 single-copy orthologs. We utilized a super-matrix approach to
335 infer a maximum likelihood (ML) species tree, based on these protein sequences. Results showed
336 statistical support for four sections of *Claviceps* with a near concordant topology to the Bayesian

337 five-gene phylogeny in Píchová *et al.* (2018). This topology was supported by neighbor-joining
338 and maximum parsimony super-matrix analyses (Additional file 1: Figure S2, S3). Notable
339 exceptions were the placement of *C. paspali* (sect. *Paspalorum*) which grouped closer to *C.*
340 *citrina* (sect. *Citrinae*) instead of sect. *Claviceps,* and *C. pusilla* which grouped closer to *C.*
341 *fusiformis* instead of *C. maximensis* (Fig. 1). We also found that sect. *Claviceps* diverged from a
342 common ancestor with sect. *Pusillae* as opposed to sect. *Paspalorum*. Our results provide
343 support for the deeply divergent lineages of sects. *Pusillae*, *Paspalorum*, and *Citrinae* with a
344 long divergent branch resulting in sect. *Claviceps* (Fig. 1).

345 Each of the 2,002 single-copy orthologs were also independently aligned and analyzed in
346 the same manner as our super-matrix phylogeny from representative isolates of each species. A
347 density consensus tree of all 2,002 topologies was concordant with our super matrix analysis but
348 reveals evidence of incongruencies, particularly within sect. *Claviceps* (Additional File 1 Fig.
349 S4) which could be caused by biological, analytical, and sampling factors (Steenwyk *et al.*
350 2019). While grouping of species generally held true to Fig. 1, variation was more related to the
351 order of branches, with *C. cyperi*, *C. arundinis*, *C. humidiphila*, and *C. perihumidiphila* showing
352 the most variability. These results indicate the presence of some incongruencies within sect.
353 *Claviceps*, sect. *Pusillae*, and across the genus (Additional File 1 Fig. S5-7) but a consensus
354 supporting our ML species tree (Fig. 1, Additional File 1 Fig. S4). There are several potential
355 causes of these incongruencies which are currently the focal point of an ongoing study.

356 To further elucidate trends of divergence within the genus we examined genomic fluidity
357 (Kislyuk *et al.* 2011) using all 82,267 orthogroups from our previous OrthoFinder analysis.
358 Genomic fluidity estimates the dissimilarity between genomes by using ratios of the number of
359 unique orthogroups to the total number of orthogroups in pairs of genomes averaged over

360 randomly chosen genome pairs from within a group on *N* genomes. For example, a fluidity value
361 of 0.05 indicates that randomly chosen pairs of genomes in a group will on average have 5%
362 unique orthogroups and share 95% of their orthogroups (Kislyuk *et al.* 2011). Section *Claviceps*,
363 which is composed of 12 different species, showed a relatively small genomic fluidity (0.0619 ±
364 0.0019) with limited variation, indicating pairwise orthogroup dissimilarity between randomly
365 sampled genomes was quite low. The amount of variation between 12 different *Claviceps* species
366 was similar to the variation between 24 *C. purpurea* s.s. isolates, however, the fluidities were
367 significantly different (Additional file 1: Table S4; $P < 0.0001$). In comparison, the fluidity of
368 sect. *Pusillae* (0.126 ± 0.014; $P < 0.0001$) was two times greater than the fluidity of sect.
369 *Claviceps* and exhibited greater variation, indicating greater dissimilarities in orthogroups
370 between randomly sampled species of sect. *Pusillae*.
371 Overall, our ML phylogeny (Fig. 1) and genome fluidity analysis (Fig. 2) indicate a large
372 evolutionary divergence separating sect. *Claviceps*. Our subsequent analyses of the genomic
373 architecture of all *Claviceps* species examine factors that could be associated with the
374 evolutionary divergence of sect. *Claviceps* and those driving cryptic speciation.
375
376 *Transposable element divergences and locations:*
377 Transposable element (TE) divergence landscapes revealed an overrepresentation of LTR
378 elements in sects. *Pusillae*, *Citrinae*, and *Paspalorum*. All three sections showed a similar large
379 peak of LTRs with divergences between 5–10% (Fig. 3; Additional file 1: Figure S8), indicating
380 a relatively recent expansion of TEs. The landscapes of sects. *Pusillae*, *Citrinae*, and
381 *Paspalorum* are in striking contrast to species of sect. *Claviceps* which showed more similar
382 abundances of LTR, DNA, LINE, SINE, and RC (helitron) elements. Species of sect. *Claviceps*

383 showed broader peaks of divergence between 5–30% but also showed an abundance of TEs with
384 ~ 0% divergence suggesting very recent TE expansion (Fig. 3; Additional file 1: Figure S8). The
385 TE landscape of *C. cyperi* showed a more striking peak of divergence between 5–10% that more
386 closely resembled the TE divergences of sects. *Pusillae*, *Paspalorum*, and *Citrinae*. However,
387 the content of the TE peak in *C. cyperi* largely contained DNA, LINE, and unclassified TEs as
388 opposed to LTR's (Additional file 1: Figure S8).

389 To identify where genes were located in relation to TEs, we calculated the average
390 distance (kbp) of each gene to the closest TE fragment. This analysis was performed for
391 predicted effectors, secreted (non-effector) genes, secondary metabolite (non-secreted) genes,
392 and all other genes. Secreted genes and predicted effectors of sects. *Claviceps* and *Pusillae*
393 species were found to be significantly closer to TEs compared to other genes within each
394 respective section (Fig. 4; $P < 0.05$), suggesting that these genes could be located in more repeat-
395 rich regions of the genome. It should be noted that we did observe a significant difference ($P <$
396 0.001, Welch's test) in TE content between sect. *Pusillae* (32.5% ± 9.59%) and sect. *Claviceps*
397 (8.79.28% ± 1.52%). In both sects. *Claviceps* and *Pusillae* secondary metabolite genes were
398 located farther away from TEs (Fig. 4; $P < 0.05$), i.e. repeat-poor regions of the genome. These
399 trends hold true for individual isolates, with a notable exception of *C. pusilla* (sect. *Pusillae*)
400 showing no significant differences in the proximity of TEs to specific gene types (Additional file
401 1: Figure S9; $P > 0.05$). Variation existed in whether particular isolates had significant
402 differences between all other genes compared to secreted genes and secondary metabolite genes,
403 but all species in sects. *Claviceps* and *Pusillae* (aside from *C. pusilla*) had predicted effector
404 genes located significantly closer to TEs (Additional file 1: Figure S9; $P < 0.05$). No significant
405 differences in the proximity of TEs to specific gene types were observed in sects. *Citrinae* and

406 *Paspalorum* (Fig. 4; $P > 0.05$), suggesting that TE's are more randomly distributed throughout
407 these genomes.
408
409 *Genome compartmentalization*:
410 To further examine genome architecture, we analyzed local gene density measured as
411 flanking distances between neighboring genes (intergenic regions) to examine evidence of
412 genome compartmentalization (i.e. clustering of genes with differences in intergenic lengths)
413 within each genome. Results showed that all 53 *Claviceps* strains exhibited a one-compartment
414 genome (lack of large-scale compartmentalization). Although, there was a tendency for more
415 genes with larger intergenic regions in sects. *Claviceps* and *Pusillae* compared to sects. *Citrinae*
416 and *Paspalorum* (Fig. 5; Additional file 1: Figure S10).
417 To further clarify evolutionary tendencies, we evaluated whether gene types showed a
418 difference in their flanking intergenic lengths compared to other genes within their genomes.
419 Results showed that predicted effector genes in sect. *Claviceps* had significantly larger intergenic
420 flanking regions compared to other genes, indicating they may reside in more gene-sparse
421 regions of the genome ($P < 0.05$, Fig. 5, Additional file 1: Figure S10). Only *C. digitariae* and *C.*
422 *lovelessi* (Additional file 1: Figure S10; $P < 0.01$, $P = 0.024$, respectively) of sect. *Pusillae* had
423 predicted effector genes with significantly l
424 arger intergenic regions than other genes, although, *C. fusiformis* and *C. pusilla* were near
425 significant (Fig. 5, Additional file 1: Figure S10; $P = 0.054$, $P = 0.056$, respectively). Flanking
426 intergenic lengths of secreted genes also showed larger intergenic lengths and were often
427 significantly larger than other genes in sect. *Claviceps* (Fig. 5; Additional file 1: Figure S10). In
428 contrast, secondary metabolite genes exhibited a widespread distribution of intergenic lengths

429 that were not significantly different than other genes in all 53 *Claviceps* strains ($P > 0.05$, Fig. 5;
430 Additional file 1: Figure S10).
431
432 *RIP analysis:*
433 To test for effects of RIP, we assessed the bi-directional similarity of genes against the
434 second closest BLASTp match within each isolate's own genome (Galagan *et al.* 2003; Urguhart
435 *et al.* 2018), supported by a BLASTp analysis against the *rid-1* RIP gene of *Neurospora crassa*,
436 and calculations of RIP indexes in 1 kb windows (500 bp increments) using The RIPper (Van
437 Wyk *et al.* 2019). Results showed that sects. *Pusillae*, *Citrinae*, and *Paspalorum* had homologs
438 of *rid-1*, fewer genes with close identity (≥ 80%), on average 27.4% ± 11.4% of their genomes
439 affected by RIP, a mean RIP composite index of -0.03 ± 0.21, and 325 ± 138 large RIP affected
440 regions (LRAR) covering 3,984 kb ± 2,144 kb of their genomes, indicating past or current
441 activity of RIP (Fig. 6; Additional file 1: Table S5, S6; Additional file 2: Table S7). This is
442 further supported by an average GC content of 42.84% ± 3.03% (Table 1) in sects. *Pusillae*,
443 *Citrinae*, and *Paspalorum*, which is on average 8.81% lower than in sect. *Claviceps* which shows
444 an absence of RIP (reported below). The presence of RIP in sects. *Pusillae*, *Citrinae*, and
445 *Paspalorum* was unexpected given the abundance of TEs within genomes of these sections
446 (Table 1; Fig. 3; Additional file 1: Figure S8) as RIP should be working to silence and inactivate
447 these TEs. While we did not directly test the activity of TEs within our genomes, due to lack of
448 RNAseq data, the peaks of low TE nucleotide divergence (<10%) in sects. *Pusillae*, *Citrinae*,
449 and *Paspalorum* (Fig. 3, Additional file 1 Figure S8) suggest recent activity of TEs
450 (Frantzeskakis *et al.* 2018).

451 In comparison, species in sect. *Claviceps* lack *rid-1* homologs, showed larger amounts of
452 gene similarity, and a general lack of evidence of RIP with only 0.13% ± 0.03% of their genomes
453 putatively affected by RIP, and a mean RIP composite index of -0.59 ± 0.01 suggesting that RIP
454 is inactive (Fig. 6; Additional file 1: Table S5, S6; Additional file 2: Table S7). Gene pairs
455 sharing a ≥80% identity to each other were often located near each other. On average 27.02% ±
456 5.91% of the pairs were separated by five or fewer genes, and 15.95% ± 3.50% of the pairs were
457 located next to each other, indicating signs of tandem gene duplication within the section
458 (Additional file 1: Table S5). *Claviceps cyperi* showed the smallest proportions of highly similar
459 tandem genes (7.77% and 5.7%) compared to other species within sect. *Claviceps*. Additional
460 variations in the proportions of highly similar tandem genes between other species of sect.
461 *Claviceps* were not evident as these proportions appeared to vary more between isolate than
462 species (Additional file 1: Table S5).
463
464 *Gene cluster expansion:*
465 The proteome of *Claviceps* genomes were used to infer orthologous gene clusters
466 (orthogroups) through protein homology and MCL clustering using OrthoFinder. Our results
467 revealed evidence of orthogroup expansion within sect. *Claviceps* as species contained more
468 genes per orthogroup than species of the other three sections (Additional file 1: Figure S11). To
469 identify the types of gene clusters that were showing putative expansion we filtered our clusters
470 by two criteria; 1) at least one isolates had two or more genes in the orthogroup, 2) there was a
471 significant difference in the mean number of genes per orthogroup between all 44 isolates in sect.
472 *Claviceps* and the 9 isolates from sects. *Pusillae*, *Citrinae*, and *Paspalorum* ($\alpha \leq 0.01$, Welch's
473 test).

474 Overall, we identified 863 (4.7%) orthogroups showing putative expansion. We observed
475 extensive expansion (orthogroups with observations of ≥ 10 genes per isolate) present in many
476 unclassified, predicted effectors, secreted (non-effector) orthogroups, and orthogroups encoding
477 genes with conserved domains (Fig. 7; Additional file 1: Figure S12, S13). Transmembrane
478 orthogroups also showed evidence of expansion with several isolates having 5-10 genes.
479 orthogroups with secondary metabolite genes showed the lowest amount of expansion (Fig. 8).
480 Overall, sect. *Claviceps* showed expansion in a greater number of orthogroups than sect.
481 *Pusillae*, *Citrinae*, and *Paspalorum* in all categories except transmembranes (Additional file 1:
482 Figure S14). Orthogroups with an average ≥ 5 genes per isolate, within sect. *Claviceps*,
483 contained a variety of functional proteins, with generally more proteins encoding
484 protein/serine/tyrosine kinase domains (Additional file 2: Table S8). Additional details can be
485 obtained from Additional file 2: Table S9 (ordered orthogroups corresponding to heatmaps; Fig.
486 7 and Additional file 1: Figure S12, S13) and Additional file 3: Table S10-1,2 (orthogroups
487 identification and functional annotation of all proteins).
488 Within sect. *Claviceps* patterns of gene counts per orthogroup appeared to break down
489 and contain variations in the number of genes per orthogroups with some presence/absences
490 occurring between isolates and species. Notably, *C. cyperi* (CCC1219) showed the lowest
491 amount of expansion, across all taxa, in comparison to other species of sect. *Claviceps*. In
492 addition, *C. spartinae* (CCC535)*, C. capensis* (CCC1504), *C. monticola* (CCC1483), *C.*
493 *pazoutovae* (CCC1485), *C. occidentalis* (LM77, 78, 84), and *C. quebecensis* (LM458, Clav32,
494 50) also showed lower expansion (Fig. 7, Additional file 1: Figure S12, S13). However, no
495 patterns were observed linking the variation in expansions with the literature determined host
496 range of different species within sect. *Claviceps*.

497

498 **Discussion:**

499 Our comparative study of 50 newly annotated genomes from four sections of *Claviceps*
500 has provided us with an enhanced understanding of evolution in the genus through knowledge of
501 factors contributing to its diversification. Our results have revealed that despite having nearly
502 identical life-strategies, these closely related species have substantially altered genomic
503 architecture and plasticity, which may drive genome adaptation. One key difference we observe
504 is a shift from characteristic aspects of one-speed genomes (i.e. less adaptable) in narrow host-
505 range *Claviceps* species (sects. *Citrinae* and *Paspalorum*) towards aspects of two-speed genomes
506 (i.e. more adaptable) in broader host-range lineages of sects. *Pusillae* and *Claviceps* (Fig. 1)
507 (Dong *et al.* 2015; Frantzeskakis *et al.* 2019).

508 The basal species of the genus, *C. citrina* (sect. *Citrinae*) and *C. paspali* (sect.
509 *Paspalorum*), are characterized by a proliferation of TEs, particularly LTRs, which do not appear
510 to be co-localized around particular gene types (Fig. 4). Coupled with a lack of large-scale
511 genome compartmentalization (Fig. 5), these two species can be considered to fit the concept of
512 a one-speed genome which are often considered to be less adaptable and potentially more prone
513 to being purged from the biota (Dong *et al.* 2015; Frantzeskakis *et al.* 2019). This could help
514 explain the paucity of section lineages and restricted host range to one grass tribe, as similar
515 patterns of large genome size, abundant TE content, and equal distribution of TEs has been
516 observed in the specialized barley pathogen *Blumeria graminis* f.sp. *hordei* (Frantzeskakis *et al.*
517 2018). Although, rapid adaptive evolution within *B. graminis* f.sp. *hordei*, has been suggested to
518 occur through copy-number variation and/or heterozygosity of effector loci (Dong *et al.* 2015;
519 Frantzeskakis *et al.* 2018, 2019). Our results show a lack of gene duplication occurring in sects.

520 *Citrinae* and *Paspalorum*, likely due to the presence of RIP. However, even with the presence of
521 RIP there was a high LTR content in these species (Fig. 3). This suggests that these LTR
522 elements have found a way to avoid RIP or indicate that these species harbor a less active
523 version of RIP as is found in several fungal species (Kachroo *et al.* 1994; Nakayashiki *et al.*
524 1999; Graïa *et al.* 2001; Ikeda *et al.* 2002; Chalyet *et al.* 2003; Kito *et al.* 2003). Nonetheless,
525 due to the high abundance of TEs (Fig. 4) and presence of RIP (Fig. 6; Additional file 1: Table
526 S5, S6), we hypothesize that aspects of RIP "leakage" could be a likely mechanism for evolution
527 in *C. citrina* and *C. paspali* (and similarly sect. *Pusillae*), as has been shown to occur in other
528 fungi (Fudal *et al.* 2009; Van de Wouw *et al.* 2010; Hane *et al.* 2015). It should be noted that
529 since the estimated divergence of sect. *Citrinae* 60.5 Mya (Píchová *et al.* 2018) it has remained
530 monotypic. It was only recently that unknown lineages of sect. *Paspalorum* were identified
531 (Oberti *et al.* 2020), although, these lineages were found on the same genera of host as *C. paspali*
532 (*Paspalum* spp.) supporting our hypothesis that species within sect. *Paspalorum* have restricted
533 host ranges. These recent findings further suggest that lack of additional lineages within these
534 sections could be due to limited records of *Claviceps* species in South America, where the genus
535 is thought to have originated (Píchová *et al.* 2018). Further research into South American
536 populations of *Claviceps* will provide significant insight into the evolution of these two sections.
537 Members of sect. *Pusillae* also exhibited a proliferation of TEs, however, as this section
538 diverged from sects. *Citrinae* and *Paspalorum* the genomic architecture evolved such that TEs
539 co-localized around predicted effector genes (Fig. 4). This proximity of TEs to effectors
540 persisted in sect. *Pusillae* species (except *C. pusilla*; Additional file 1: Figure S9) and sect.
541 *Claviceps* species potentially resulting in the large intergenic regions flanking predicted effector
542 genes (Fig. 5, Additional file 1: Figure S10). Together, these genomic alterations indicate aspects

543 of a two-speed genome (Dong *et al.* 2015; Möller & Stukenbrock 2017). We hypothesize that
544 these observed genomic changes influenced the divergence and adaptability of sects. *Pusillae*
545 and *Claviceps* (Fig. 1) (Raffaele & Kamoun 2012; Stukenbrock 2013; Möller & Stukenbrock
546 2017).

547 Furthermore, our analyses suggest that the divergence of sect. *Claviceps*, from sect.
548 *Pusillae*, is associated with a loss of RIP (Fig. 1, 6; Additional file 1: Table S6). In the absence
549 of RIP, the gene-sparse regions rich in TEs and effectors could be hot spots for duplication,
550 deletion, and recombination (Galagan *et al.* 2003, 2004; Raffaele & Kamoun 2012; Dong *et al.*
551 2015; Faino *et al.* 2016; Möller & Stukenbrock 2017; Frantzeskakis *et al.* 2018, 2019). This
552 would explain the observations of tandem gene duplication within the section (Fig. 6, 7;
553 Additional file 1: Table S5, Figure S11-S14), which may facilitate rapid speciation, as has been
554 postulated in several smut fungi (Kämper *et al.* 2006; Schirawski *et al.* 2010; Dutheil *et al.*
555 2016). In fact, *C. cyperi*, a basal species of sect. *Claviceps* and thought to be ancestral from
556 ancestral state reconstructions of host range (Píchová *et al.* 2018), showed the least amount of
557 gene cluster expansion and tandem duplication (Fig. 7; Additional file 1: Table S5, Figure S12,
558 S13). Potentially indicating that gene duplication is contributing to the divergence of new
559 species, as other species in sect. *Claviceps* have increased genome size, gene count, and number
560 of closely related gene pairs (≥80% identity) (Table 1; Additional file 1 Table S5). Within sect.
561 *Claviceps* gene duplication is likely facilitated by recombination events during annual sexual
562 reproduction (Esser & Tudzynski 1978). Future studies on recombination will be critical to our
563 understanding of the mechanisms driving gene duplication and elucidating factors associated
564 with the observations of potential incomplete lineage sorting (Pease & Hahn 2013) within the
565 section.

566 Substantially altered genomic architecture and plasticity between *Claviceps* sections was
567 observed in this study, yet it is unclear whether the evolution of these genomes were caused by
568 contact with new hosts and different climates as ancestral lineages migrated out of South
569 America (Píchová *et al.* 2018), or if the evolution towards a two-speed genome provided an
570 advantage in adapting to new hosts or environments. Further research is needed to clarify this
571 point. As sects. *Pusillae* and *Claviceps* have larger host ranges (5 tribes and 13 tribes,
572 respectively) and increased levels of speciation (Píchová *et al.* 2018), they represent ideal
573 systems to test this hypothesis. It is postulated that sect. *Pusillae* was transferred to Africa (ca
574 50.3 Mya), while sect. *Claviceps* originated in North America (ca. 20.7 Mya), and it is likely that
575 the common ancestor shared between these sections (Fig. 1) had strains that were transferred to
576 Africa, likely due to insect vectors via transatlantic long-distance dispersal (Píchová *et al.* 2018).
577 The strains that remained, in South America, likely persisted but appeared to not speciate for
578 roughly 30 Mya (Píchová *et al.* 2018), despite having aspects of a more adaptable two-speed
579 genome (Fig. 4, 5). Limited sampling records could be a factor contributing to this lack of
580 speciation during this 30 My period, but it could also be suggested that the ancestral species of
581 sects. *Claviceps* did not diverge due to a lack of diversification of host species (Píchová *et al.*
582 2018). It is well known that *Claviceps* species share a rather unique relationship with their hosts
583 (strict ovarian parasites). The evolution of *Claviceps* appears to be primarily driven by the
584 evolution and diversification of the host species (Píchová *et al.* 2018). This can be inferred from
585 divergence time estimates which show that the crown node of sect. *Pusillae* aligns with the
586 crown node of PACMAD grasses (ca. 45 Mya) (Bouchenak-Khelladi *et al.* 2010, Píchová *et al.*
587 2018), suggesting that these two organisms radiated in tandem after ancestral strains of sect.
588 *Pusillae* were transferred to Africa. Similarly, the estimated crown node of sect. *Claviceps*

589 corresponds with the origin of the core Pooideae (Poeae, Triticeae, Bromeae, and Littledaleae),
590 which occurred in North America (ca. 33-26 Mya) (Bouchenak-Khelladi *et al.* 2010; Sandve &
591 Fjellheim 2010).

592 Such a large difference between the estimate divergence age (~30 My) and long
593 divergence branch (Fig. 1) between sect. *Clavcieps* and the other three sections (Píchová *et al.*
594 2018) suggests that a sudden event sparked the adaptive radiation within this section (Fig. 1).
595 Under an assumption that ancestral strains of sect. *Claviceps* were infecting sedges (Cyperaceae),
596 as is seen in the basal species *C. cyperi*, a host jump to BOP grasses could have ignited the rapid
597 speciation of sect. *Claviceps*, similar to the suggested tandem radiation of sect. *Pusillae* with the
598 PACMAD grasses in Africa. However, unknown factors might be responsible for the drastic
599 genomic changes (i.e. putative loss of RIP) observed in sect. *Claviceps*, as no such changes were
600 observed in sect. *Pusillae*. The radiation of the core Pooideae occurred after a global super-
601 cooling period (ca. 33-26 Mya) in North America. During this period, Pooideae experienced a
602 stress response gene family expansion which enabled adaptation and diversification to cooler,
603 more open, habitats (Kellogg 2001; Sandve & Fjellheim 2010). As gene cluster expansion was
604 observed in sect. *Claviceps* (the only section to infect BOP grasses) it suggests that the same
605 environmental factors that caused the radiation of Pooideae could have similarly affected sect.
606 *Claviceps* (Kondrashov 2012) and might have resulted in the host jump to Pooideae, and
607 potentially other BOP tribes. Interestingly, one of the orthogroups significantly expanded in sect.
608 *Claviceps* (OG0000016) contains proteins associated with a cold-adapted (Alias *et al.* 2014)
609 serine peptidase S8 subtilase (MER0047718; S08.139) (Additional file 2: Table S8). Although
610 the crown node of sect. *Claviceps* is estimated at approximately 5-10 My before the radiation of

611 the core Pooideae, the 95% highest posterior density determined in Píchová *et al.* (2018) could
612 indicate both radiation events occurred at similar times.
613 Further examination of *Claviceps* species in South and Central America needs to be
614 conducted to better elucidate the evolution and dispersal of the genus (Píchová *et al.* 2018).
615 Efforts should focus on the elusive *C. junci*, a pathogen of Juncaceae (rushes), which is thought
616 to reside in sect. *Claviceps* based on morphological and geographic characteristics (Langdon
617 1952; Píchová *et al.* 2018). This species, and potentially others, will provide further insight into
618 the early evolution of sect. *Claviceps* and could bridge the current gap between the
619 environmental factors that sparked the radiation of the core Pooideae and sect. *Claviceps*.
620

621 **Acknowledgements:**
622 We thank Dr. Miroslav Kolařík for providing *Claviceps* isolates from the Culture
623 Collection of Clavicipitaceae at Institute of Microbiology, Academy of Sciences of the Czech
624 Republic (CCC samples); Parivash Shoukouhi, Dr. Jim Menzies, and Zlatko Popovic for
625 collection, isolation, maintenance, and DNA extraction of LM samples; Dr. Chris Schardl and
626 Dr. Neil Moore, University of Kentucky, for providing the 2013 GFF3 files for *C. paspali* and *C.*
627 *fusiformis*; Dr. Joshua Weitz and the Franklin Graybill Statistical Laboratory at Colorado State
628 University for their help in data analysis of genomic fluidity; Molecular Technologies
629 Laboratory (MTL) at the Ottawa Research & Development Centre, Agriculture and Agri-Food
630 Canada, especially Kasia Dadej for technical assistance. For genomes downloaded from JGI
631 these sequence data were produced by the US Department of Energy Joint Genome
632 Institute https://www.jgi.doe.gov/ in collaboration with the user community.
633

Funding:

This work is supported by the Agriculture and Food Research Initiative (AFRI) National Institute of Food and Agriculture (NIFA) Fellowships Grant Program: Predoctoral Fellowships grant no. 2019-67011-29502/project accession no. 1019134 from the United States Department of Agriculture (USDA), and by the American Malting Barley Association grant no. 17037621. Dr. Broders is supported by the Simon's Foundation Grant number 429440 to the Smithsonian Tropical Research Institute. Whole-genome sequencing of LM samples was supported, in part, by funding provided to Dr. Jeremy Dettman from Agriculture and Agri-Food Canada's Biological Collections Data Mobilization Initiative (BioMob, Work Package 2, project J-001564).

Data availability:

Datasets and scripts are available on Dryad: Wyka, Stephen *et al.* (2020), Genus-wide comparison reveals divergence and evolution of the four sections within the genus Claviceps are the result of varying mechanisms driving genome evolution and host range, Dryad, Dataset, https://doi.org/10.5061/dryad.18931zcsk. (Submitted upon publication)

Genomes and Illumina raw reads were deposited to NCBI under the BioProject PRJNA528707 (Additional file 1: Table S1). Scripts are maintained within the GitHub repository of the primary author's, https://github.com/PlantDr430/CSU_scripts. TransposableELMT can be found at Zenodo doi: 105281/zenodo3469661. All phylogenetic trees were made available at TreeBase (ID:XXXX).

Author Contributions:

657 The project was conceived and designed by S.A.W., S.J.M., and K.B.; S.A.W. performed
658 the research, annotations, bioinformatic workflows, and analyzed the data with technical
659 troubleshooting from S.J.M.; M.L. and J.R.D initiated whole-genome sequencing of LM
660 samples; M.L., V.N., and K.B. provided management, research advice, and editorial
661 contributions; S.A.W. wrote the paper with contributions from all other authors.
662

663 **References:**

664 Alderman SC, Halse RR, White JF. 2004. A reevaluation of the host range and geographical
665 distribution of *Claviceps* species in the United States. *Plant Disease* 88:63–81.

666 Alias N, Ahmad Mazian M, Salleh AB, Basri M, Rahman RN. 2014. Molecular cloning and
667 optimization for high level expression of cold-adapted serine protease from Antarctic yeast
668 *Glaciozyma antarctica* PI12. *Enzyme Research* 2014:197938.

669 Andrews S. 2010. FastQC: a quality control tool for high throughput sequence data. Available
670 online at: http://wwwbioinformaticsbabrahamacuk/projects/fastqc.

671 Bao W, Kojima KK, Kohany O. 2015. Repbase Update, a database of repetitive elements in
672 eukaryotic genomes. *Mobile DNA* 6:11.

673 Berriman M, Coghlan A, Tsai IJ. 2018. Creation of a comprehensive repeat library for newly
674 sequenced parasitic worm genome. *Protocol Exchange* doi: 101038/protex2018054.

675 Blanco E, Parra G, Guigo R. 2007. Using geneid to identify genes. *Current Protocols in*
676 *Bioinformatics* 18:431-4328.

677 Blin K, Shaw S, Steinke K, Villebro R, Ziemert N, Lee SY, Medema MH, Weber T. 2019.
678 antiSMASH 5.0: updates to the secondary metabolite genome mining pipeline. *Nucleic Acids*
679 *Research* 47:W81-87.

680 Bolger AM, Lohse M, Usadel B. 2014. Trimmomatic: a flexible trimmer for Illumina sequence
681 data. *Bioinformatics* 30:2114-20.
682 Bouchenak-Khelladi Y, Verboom GA, Savolainen V, Hodkinson TR. 2010. Biogeography of the
683 grasses Poaceae: a phylogenetic approach to reveal evolutionary history in geographical
684 space and geological time. *Botanical Journal of the Linnean Society* 162:543–557.
685 Bouckaert R, Heled J. 2014. DensiTree 2: Seeing Trees Through the Forest, doi:
686 http://dx.doi.org/10.1101/012401.
687 Buchfunk B, Xie C, Huson DH. 2015. Fast and sensitive protein alignment using DIAMOND.
688 *Nature Methods* 12:59-60.
689 Bushnell, B. 2014. BBMap: A fast, accurate, splice-aware aligner. Available at:
690 https://sourceforgenet/projects/bbmap/.
691 Campbell, W.P. 1957. Studies on ergot infection in gramineous hosts. *Canadian Journal of*
692 *Botany* 35:315-320.
693 Cantu D, Segovia V, MacLean D, Bayles R, Chen X, Kamoun S, Dubcovsky J, Saunders DGO,
694 Uauy C. 2013. Genome analyses of the wheat yellow stripe rust pathogen *Puccinia*
695 *striiformis* f sp *tritici*reveal polymorphic and haustorial expressed secreted proteins as
696 candidate effectors. *BMC Genomics* 14:270.
697 Castresana J. 2000. Selection of conserved blocks from multiple alignments for their use in
698 phylogenetic analysis. *Molecular Biology and Evolution* 17:540-552.
699 Chalvet F, Grimaldi C, Kaper F, Langin T, Dabousii MJ. 2003. Hop, an active Mutator-like
700 element in the genome of the fungus *Fusarium oxysporum. Molecular Biology and Evolution*
701 20:1362–1375.

702 Dong S, Raffaele S, Kamoun S. 2015. The two-speed genomes of filamentous pathogens: waltz
703 with plants. *Current Opinion in Genetics and Development* 35:57–65.
704 Doyle JJ, Doyle JL. 1987. A rapid DNA isolation procedure for small quantities of fresh leaf
705 tissue. *Phytochemical Bulletin* 19:11-15.
706 Dutheil JY, Mannhaupt G, Schweizer G, Sieber CMK, Münsterkötter M, Güldener U,
707 Schirawski J, Kahmann R. 2016. A tale of genome compartmentalization: the evolution of
708 virulence clusters in smut fungi. *Genome Biology and Evolution* 8:681–704.
709 Edgar RC. 2010. Search and clustering orders of magnitude faster than BLAST. *Bioinformatics*
710 26:2460-2461.
711 Ellinghaus D, Kurtz S, Willhoeft U. 2008. LTRharvest, a efficient and flexible software for de
712 novo detection of LTR retrotransposons. *BMC Bioinformatics* 9:18.
713 Emms DM, Kelly S. 2019. OrthoFinder: phylogenetic orthology inference for comparative
714 genomics. *Genome Biology* 20:238.
715 Esser K, Tudzynski P. 1978. Genetics of the ergot fungus *Claviceps purpurea*. *Theoretical and*
716 *Applied Genetics* 53:145-149.
717 Estep LK, Torriani SFF, Zala M, Anderson NP, Flowers MD, McDonald BA, Mundt CC,
718 Brunner PC. 2015. Emergence and early evolution of fungicide resistance in North American
719 populations of *Zymoseptoria tritici*. *Plant Pathology* 64:961-971.
720 Faino L, Seidl MF, Shi-Kunne X, Pauper M, van den Berg GCM, Wittenberg AHJ, Thomma
721 BPHJ. 2016. Transposons passively and actively contribute to evolution of the two-speed
722 genome of a fungal pathogen. *Genome Research* 26:1091–1100.

723 Fisher AJ, DiTomaso JM, Gordon TR, Aegerter BJ, Ayres DR. 2007. Salt marsh *Claviceps*
724 *purpurea* in native and invaded Spartina marshes in Northern California. *Plant Disease*
725 91:380–386.
726 Frantzeskakis L, Kracher B, Kusch S, *et al.* 2018 .Signatures of host specialization and a recent
727 transposable element burst in the dynamic one-speed genome of the fungal barley powdery
728 mildew pathogen. *BMC Genomics* 19:381.
729 Frantzeskakis L, Kusch S, Panstruga R 2019. The need for speed: compartmentalized genome
730 evolution in filamentous phytopathogens. *Molecular Plant Pathology* 20:3-7
731 Freitag M, Williams RL, Kothe GO, Selker EU. 2002. A cytosine methyltransferase homologue
732 is essential for repeat_induced point mutation in *Neurospora crassa*. *PNAS* 99:8802-8807.
733 Fudal I, Ross S, Brun H, Besnard A-L, Ermel M, Kuhn M-L, Balesdent M-H, Rouxel T. 2009.
734 Repeat-induced point mutation RIP as an alternative mechanism of evolution towards
735 virulence in *Leptosphaeria maculans*. *Molecular Plant-Microbe Interactions* 22:932-941.
736 Galagan JE, Selker EU. 2004. RIP: the evolutionary cost of genome defense. *TRENDS in*
737 *Genetics* 20:417-423.
738 Galagan JE, Calvo SE, Borkovich KA *et al*. 2003. The genome sequence of the filamentous
739 fungus *Neurospora crassa*. *Nature* 422:859-868.
740 Gladieux P, Ropars J, Badouin H, *et al.* 2014. Fungal evolutionary genomics provides insight
741 into the mechanisms of adaptive divergence in eukaryotes. *Molecular ecology* 23:753-773.
742 Grabherr MG, Haas BJ, Yassour M, *et al.* 2011 Full-length transcriptome assembly from RNA-
743 seq data without a reference genome. *Nature Biotechnology* 29:644-52.

744 Graïa F, Lespinet O, Rimbault B, Deguard-Chablat M, Coppin E, Picard M. 2001. Genome
745 quality control: RIP repeat-induced point mutation comes to *Podospora*. *Molecular*
746 *Microbiology* 40:586–595.
747 Grandaubert J, Bhattacharyya A, Stukenbrock EH. 2015. RNA-seq-based gene annotation and
748 comparative genomics of four fungal grass pathogens in the genus *Zymoseptoria* identify
749 novel orphan genes and species-specific invasions of transposable elements. *Genes,*
750 *Genomics, Genetics* 5:1323-1333.
751 Grandaubert J, Dutheil JY, Stukenbrock EH. 2019. The genomic determinants of adaptive
752 evolution in a fungal pathogen. *Evolution Letters* 3:299-312.
753 Gu Z, Eils R, Schlesner M. 2016. Complex heatmaps reveal patterns and correlations in
754 multidimensional genomic data. *Bioinformatics* 32:2847-9.
755 Hane JK, Williams AH, Taranto AP, Solomon PS, Oliver RP. 201.5 Repeat-induced point
756 mutation: a fungal-specific, endogenous mutagenesis process. In: van den Berg MA
757 Maruthachalam K, editors. *Genetic transformation systems in fungi*. Vol. 2. Springer
758 International Publishing, p. 55-68.
759 Hass B. 2010. TransposonPSI. Available online at: http://transposonpsisourceforgenet.
760 Hass BJ, Salzberg SL, Zhu W, Pertea M, Allen JE, Orvis J, White O, Buell CR, Wortman JR.
761 2008. Automated eukaryotic gene structure annotation using EVidenceModeler and the
762 program to assemble spliced alignments. *Genome Biology* 9:R7.
763 Hinsch J, Galuszka P, Tudzynski P. 2016. Functional characterization of the first filamentous
764 fungal tRNA-isopentenyltransferase and its role in the virulence of *Claviceps purpurea*. *New*
765 *Phytologist* 211:980-992.

766 Hinsch J, Vrabka J, Oeser B, Novák O, Galuszka P, Tudzynski P. 2015. *De novo* biosynthesis of
767 cytokinins in the biotrophic fungus *Claviceps purpurea*. *Environmental Microbiology*
768 17:2935-2951.
769 Huerta-Cepas J, Szklarczyk D, Jensen LJ, von Mering C, Bork P. 2016. Fast genome-wide
770 functional annotation through orthology assignment by eggnog-mapper. *Molecular Biology*
771 *and Evolution* 34:2115-2122.
772 Huerta-Cepas J, Szklarczyk D, Heller D, *et al.* 2019. eggnog 5.0: a hierarchical, functionally and
773 phylogenetically annotated orthology resource based on 5090 organisms and 2502 viruses.
774 *Nucleic Acids Research* 47:D309-314
775 Ikeda K, Nakayashiki H, Tosa Y, Mayama S. 2002. Repeat-induced point mutation RIP in
776 *Magnaporthe grisea*: implications for its sexual cycle in the natural field context. *Molecular*
777 *Microbiology* 45:1355–1364.
778 Jones P, Binns D, Chang H-Y, *et al.* 2014. InterProScan 5: genome-scale protein function
779 classification. *Bioinformatics* 30:1236-1240.
780 Jungehülsing U, Tudzynski P. 1997. Analysis of genetic diversity in *Claviceps purpurea* by
781 RAPD markers. *Mycological Research* 101:1–6.
782 Kachroo P, Leong SA, Chatto BB. 1994. Pot2, an inverted repeat transposon from the rice blast
783 fungus *Magnaporthe grisea*. *Molecular and General Genetics* 245:339–348.
784 Käll L, Krogh A, Sonnhammer EL. 2007. Advantages of combined transmembrane topology and
785 signal peptide prediction--the Phobius web server. *Nucleic Acids Research* 35:W429-32.
786 Kämper J, Kahmann R, Bölker M *et al.* 2006. Insights from the genome of the biotrophic fungal
787 plant pathogen *Ustilago maydis*. *Nature* 444:97–101.

788 Katoh K, Standley, DM. 2013. MAFFT multiple sequence alignment software version 7:
789 improvements in performance and usability. *Molecular Biology and Evolution* 30, 772-780.
790 Keilwagen J, Wenk M, Erickson JL, Schattat MH, Grau J, Hartung F. 2016. Using intron
791 position conservation for homology-based gene prediction. *Nucleic Acids Research* 44:e89.
792 Kellogg, EA. 2001. Evolutionary history of the grasses. *Plant Physiology* 125:1198-1205.
793 Kind S, Schurack S, Hinsch J, Tudzynski P. 2018a. Brachypodium distachyon as alternative
794 model host system for the ergot fungus *Claviceps purpurea*. *Molecular Plant Pathology*
795 19:1005-1011.
796 Kind S, Hinsch J, Vrabka J, Hradilová M, Majeská-Čudejková M, Tudzynski P, Galuska P.
797 2018b. Manipulation of cytokinin level in the ergot fungus *Claviceps purpurea* emphasizes
798 its contribution to virulence. *Current Genetics* 64:1303-1319.
799 Kiran K, Rawal HC, Dubey H, *et al.* 2016. Draft genome of the wheat rust pathogen *Puccinia*
800 *triticina* unravels genome-wide structural variations during evolution. *Genome Biology and*
801 *Evolution* 8:2702-2721.
802 Kiran K, Rawal HC, Dubey H, Jaswal R, Bhardwaj SC, Prasad P, Pal D, Devanna BN, Sharma
803 TR. 2017. Dissection of genomic features and variations of three pathotypes of *Puccinia*
804 *striiformis* through whole genome sequencing. *Scientific Reports* 7:42419.
805 Kislyuk AO, Haegeman B, Bergman NH, Weitz JS. 2011. Genomic fluidity: an integrative view
806 of gene diversity within microbial populations. *BMC Genomics* 12:32.
807 Kito H, Takahashi Y, Sato J, Fukiya S, Sone T, Tomita F. 2003. Occan, a novel transposon in the
808 Fot1 family, is ubiquitously found in several *Magnaporthe grisea* isolates. *Current Genetics*
809 42:322–331.

810 Kondrashov FA. 2012. Gene duplication as a mechanism of genomic adaptation to a changing
811 environment. *Proceedings of the Royal Society B* 279:5048-5057.
812 Korf I. 2004. Gene finding in novel Genomes. *BMC Bioinformatics* 5:59.
813 Krogh A, Larsson B, von Heijne G, Sonnhammer ELL. 2001. Predicting transmembrane protein
814 topology with a hidden markov model: application to complete genomes. *Journal of*
815 *Molecular Biology* 305:567-580.
816 Kvas M, Marasas WFO, Wingfield BD, Wingfield MJ, Steenkamp ET. 2009. Diversity and
817 evolution of *Fusarium* species in the *Gibberella fujikuroi* complex. *Fungal Diversity* 34:1-
818 21.
819 Langdon RFN. 1952. Studies on ergot PhD thesis. Queensland University, Brisbane, Australia
820 Li H. 2018. Minimap2: pairwise alignment for nucleotide sequences. *Bioinformatics* 34:3094-
821 3100.
822 Ma L-J, van der Does HC, Borkovich KA, *et al*. 2010. Comparative genomics reveals mobile
823 pathogenicity chromosomes in *Fusarium*. *Nature* 464:367-373.
824 Majoros WH, Pertea M, Salzberg SL. 2004. TigrScan and GlimmerHMM: two open-source ab
825 initio eukaryotic gene-finders. *Bioinformatics* 20:2878-2879.
826 Mario S, Diekhans M, Baertsch R, Haussler D. 2008. Using native and syntenically mapped
827 cDNA alignments to improve *de novo* gene finding. *Bioinformatics* 24:637–644.
828 Möller M, Stukenbrock EH. 2017. Evolution and genome architecture in fungal plant pathogens.
829 *Nature Reviews Microbiology* 15:756-771.
830 Nakayashiki H, Nishimoto N, Ikeda K, Tosa Y, Mayama S. 1999. Degenerate MAGGY elements
831 in a subgroup of *Pyricularia grisea*: a possible example of successful capture of a genetic
832 invader by a fungal genome. *Molecular and General Genetics* 261:958–966.

833 Newton RR, Newton IL. 2013. PhyBin: binning trees by topology. *Peer J.* 1:e187; doi:
834 10.7717/peerj.187.
835 Nielsen H. 2017. Predicting secretory proteins with SignalP In: *Protein function prediction* eds.
836 Kihara D. *Methods in Molecular Biology* 1611 Humana Press, New York, NY.
837 Nurk S, Bankevich A, Antipov D, *et al.* 2013. Assembling genomes and mini-metagenomes from
838 highly chimeric reads. *Research in Computational Molecular Biology RECOMB 2013*
839 *Lecture Notes in Computer Science*, vol 7821 Springer, Berlin, Heidelberg.
840 Oberti H, Dalla Rizza M., Reyno R, Murchio S, Altier N, Abreo E. 2020. Diversity of *Claviceps*
841 *paspali* reveals unknown lineages and unique alkaloid genotypes. *Mycologia* 112:1-14.
842 Oeser B, Kind S, Schurack S, Schmutzer T, Tudzynski P, Hinsch J. 2017. Cross-talk of the
843 biotrophic pathogen *Claviceps purpurea* and its host *Secale cereale*. *BMC Genomics* 18:273.
844 Palmer J, Stajich J. 2019. nextgenusfs/funannotate: funannotate v1.6.0 Version 1.6.0 Zenodo doi:
845 105281/zenodo3354704.
846 Pease JB, Hahn MW. 2013. More accurate phylogenies inferred from low-recombination regions
847 in the presence of incomplete lineage sorting. *Evolution* 67:2376-2384.
848 Píchová K, Pažoutová S, Kostovčík M, Chudíčková M, Stodulůkvá E, Novák P, Flieger M, van
849 der Linde E, Kolařík M. 2018. Evolutionary history of ergot with a new infrageneric
850 classification Hypocreales: Clavicipitaceae: *Claviceps*. *Molecular Phylogenetics and*
851 *Evolution* 123:73-87.
852 Poppe S, Dorcheimer L, Happel P, Stukenbrock EH. 2015. Rapidly evolving genes are key
853 players in host specialization and virulence of the fungal wheat pathogen *Zymoseptoria tritici*
854 *Mycosphaerella graminicola*. *PLoS Pathogens* 11:e1005055.

855 Price MN, Dehal PS, Arkin AP. 2010. FastTree 2 – approximately maximum-likelihood trees for
856 large alignments. *PLoS ONE* 5:e9490.
857 Raffaele S, Kamoun S. 2012. Genome evolution in filamentous plant pathogens: why bigger can
858 be better. *Nature Reviews Microbiology* 10:417–430.
859 Raybould AF, Gray AJ, Clarke RT. 1998. The long-term epidemic of *Claviceps purpurea* on
860 *Spartina anglica* in Poole Harbour: pattern of infection, effects on seed production and the
861 role of *Fusarium heterosporum*. *New Phytologist* 138:497–505.
862 Rep M, Kistler HC. 2010. The genomic organization of plant pathogenicity in *Fusarium* species.
863 *Current Opinion in Plant Biology* 13:420-426.
864 Sandve SR, Fjellheim S. 2010. Did gene family expansions during the Eocene- Oligocene
865 boundary climate cooling play a role in Pooideae adaptation to cool climates? *Molecular*
866 *Ecology* 19:2075–2088.
867 Schardl CL, Young CA, Hesse U, *et al*. 2013. Plant-symbiotic fungi as chemical engineers:
868 multi-genome analysis of the Clavicipitaceae reveals dynamics of alkaloid loci. *PLoS*
869 *Genetics* 9:e1003323.
870 Schirawski J, Mannhaupt G, Münch K *et al.* 2010. Pathogenicity determinants in smut fungi
871 revealed by genome comparison. *Science* 330:1546–1548.
872 Smit AFA, Hubley R. 2015. RepeatModeler Open-10. Available online at:
873 http://wwwrepeatmaskerorg.
874 Smit AFA, Hubley R, Green P. 2015. RepeatMasker Open-40. Available online at:
875 http://wwwrepeatmaskerorg.

876 Soreng RJ, Peterson PM, Romaschenko K, *et al.* 2017. A worldwide phylogenetic classification
877 of the Poaceae Gramineae II: An update and a comparison of two 2015 classifications.
878 *Journal of Systematics and Evolution* 55:259–290.
879 Sperschneider J, Gardiner DM, Thatcher LF, Lyons R, Singh KB, Manners JM, and Taylor JM.
880 2015. Genome-wide analysis in three *Fusarium* pathogens identifies rapidly evolving
881 chromosomes and genes associated with pathogenicity. *Genome Biology and Evolution*
882 7:1613-1627.
883 Sperschneider J, Dobbs PN, Gardiner DM, Singh KB, Taylor JM. 2018. Improved prediction of
884 fungal effector proteins from secretomes with EffectorP 2.0. *Molecular Plant Pathology*
885 19:2094-2110.
886 Steenwyk JL, Shen X-X, Lind AL, Goldman GH, Rokas A. 2019. A robust phylogenomic time
887 tree for biotechnologically and medically important fungi in the genera *Aspergillus* and
888 *Penicillium*. *MBio* 10:e00925-19.
889 Steinbiss S, Willhoeft U, Gremme G, Kurtz S. 2009. Fine-grained annotation and classification
890 of *de novo* predicted LTR retrotransposons. *Nucleic Acids Research* 37:7002–7013.
891 Stukenbrock EH. 2013. Evolution, selection and isolation: a genomic view of speciation in
892 fungal plant pathogens. *New Phytologist* 199:895–907.
893 Stukenbrock EH, Dutheil JY. 2018. Fine-scale recombination maps of fungal plant pathogens
894 reveal dynamic recombination landscape and intragenic hotspots. *Genetics* 208:1209-1229.
895 Sudhir K, Stecher G, Li M, Knyaz C, Tamura K. 2018. MEGA X: Molecular Evolutionary
896 Genetics Analysis across computing platforms. *Molecular Biology and Evolution* 35:1547-
897 1549.

898 Ter-Hovhannisyan V, Lomsadze A, Chernoff YO, Borodovsky M. 2008. Gene prediction in
899 novel fungal genomes using an ab initio algorithm with unsupervised training. *Genome*
900 *Research* 18:1979-1990.
901 Testa A, Hane JK, Ellwood SR, Oliver RP. 2015. CodingQuarry: highly accurate hidden markov
902 model gene prediction in fungal genomes using RNA-seq transcripts. *BMC Genomics*
903 16:170.
904 Testa A, Oliver R, Hane J. 2015. Overview of genomic and bioinformatic resources for
905 *Zymoseptoria tritici*. *Fungal Genetics and Biology* 79:13-16.
906 Tudzynski P, Scheffer JAN. 2004. *Claviceps purpurea*: molecular aspects of a unique
907 pathogenic lifestyle. *Molecular Plant Pathology 5*:377-388.
908 Urguhart AS, Mondo SJ, Makela MR *et al.* 2018. Genomic and genetic insights into a
909 cosmopolitan fungus, *Paecilomyces variotii* Eurotiales. *Frontiers in Microbiology* 9:3058.
910 Van de Wouw AP, Cozijnsen AJ, Hane JK, Brunner PC, McDonald BA, Oliver RP, Howlett BJ.
911 2010. Evolution of linked avirulence effectors in *Leptosphaeria maculans* is affected by
912 genomic environment and exposure to resistance genes in host plants. *PLoS Pathogens*
913 6:e1001180.
914 Van Wyk S, Harrison CH, Wingfield BD, De Vos L, van Der Merwe NA, Steenkamp, ET. 2019.
915 The RIPper, a web-based tool for genome-wide quantification of Repeat-Induced Point RIP
916 mutations. *PeerJ* 7:e7447.
917 Wäli PP, Wäli PR, Saikkonen K, Tuomi J. 2013. Is the pathogenic ergot fungus a conditional
918 defensive mutualist for its host grass? *PLoS ONE* 8:e69249.

919 Watanabe M, Yonezawa T, Lee K, Kumagai S, Sugita-Konishi Y, Goto K, Hara-Kudo Y. 2011.
920 Molecular phylogeny of the higher and lower taxonomy of the *Fusarium* genus and
921 differences in the evolutionary histories of multiple genes. *BMC Evol Biol* 11:322.
922 Waterhouse RM, Seppey M, Simao FA, Manni M, Ioannidis P, Klioutchnikov G, Kriventseva
923 EV, Zdobnov EM. 2018. BUSCO applications from quality assessments to gene prediction
924 and phylogenomics. *Molecular Biology and Evolution* 35:543-548.
925 Wingfield BD, Miao L, Nguyen HDT, *et al.* 2018. Nine draft genome sequences of *Claviceps*
926 *purpurea* s.lat., including *C. arundinis*, *C. humidiphila*, and *C.* cf. *spartinae*,
927 pseudomolecules for the pitch canker pathogen *Fusarium circinatum*, draft genome of
928 *Davidsoniella eucalypti*, *Grosmannia galeiformis*, *Quambalaria eucalypti*, and
929 *Teratosphaeria destructans*. *IMA Fungus* 9:401-418.
930 Wu B, Macielog AI, Hao W. 2017. Origin and spread of spliceosomal introns: insights from the
931 fungal clade *Zymoseptoria*. *Genome Biology and Evolution* 9:2658-2667.
932 Xu Z, Wang H. 2007. LTR_FINDER: an efficient tool for the prediction of full-length LTR
933 retrotransposons. *Nucleic Acids Research* 35:W265–268.
934
935 **Figure Captions:**
936
937 **Figure 1:** Maximum likelihood phylogenetic reconstruction of the *Claviceps* genus using amino
938 acid sequences of 2,002 single copy orthologs with 1000 bootstrap replicates. Pink dots at
939 branches represent bootstrap values ≥95. Arrows and descriptions indicate potential changes in
940 genomic architecture between *Claviceps* sections identified in this study.
941

942 **Figure 2:** Genomic fluidity (dashed lines) for specified groups within the order Hypocreales.
943 Species level groups contain multiple isolates of a given species, while section and genus level
944 groups contain one strain from representative species to remove phylogenetic bias. Shaded
945 regions represent standard error and were determined from total variance, containing both the
946 variance due to the limited number of samples genomes and the variance due to subsampling
947 within the sample of genomes. Letters correspond to significant difference between fluidities
948 determined through a two-sided two-sample z-test ($P < 0.05$; Additional file 1: Table S4).
949 Legend is in descending order based on fluidity, and names are additionally appended to mean
950 lines for clarity.
951
952 **Figure 3:** Transposable element (TE) fragment divergence landscapes for representative species
953 of each *Claviceps* section; *C. purpurea* 20.1 (sect. *Claviceps*), *C. maximensis* CCC398 (sect.
954 *Pusillae*), *C. paspali* RRC1481 (sect. *Paspalorum*), and *C. citrina* (sect. *Citrinae*). Stacked bar
955 graphs show the non-normalized sequence length occupied in each genome (y-axis) for each TE
956 type based on their percent divergence (x-axis) from their corresponding consensus sequence.
957 Landscape for all remaining isolates can be seen in Additional file 1: Figure S8.
958
959 **Figure 4:** Boxplot distributions of predicted effectors, secreted (non-effectors), secondary
960 metabolite (non-secreted) genes and other genes (i.e. genes that are not effectors, secreted, or
961 secondary (2°) metabolite genes) in *Claviceps* sections showing the mean distance (kbp) of each
962 gene to the closest transposable element fragment (5' and 3' flanking distances were averaged
963 together). Kruskal Wallis (*P*-value; * < 0.05, ** < 0.01, *** < 0.001, n.s. = not significant).
964 Pairwise comparison was performed with Mann-Whitney U-test with Benjamini-Hochberg

965 multi-test correction. Letters correspond to significant differences between gene categories
966 within sections ($P < 0.05$). Plots for all individual isolates can been seen in Additional file 1:
967 Figure S9.
968
969 **Figure 5:** Gene density as a function of flanking 5' and 3' intergenic region size (y- and x-axis)
970 of representative isolates of each of the four sections within the *Claviceps* genus; *C, purpurea*
971 20.1 (sect. *Claviceps*), *C. maximensis* CCC398 (sect. *Pusillae*), *C. paspali* RRC1481 (sect.
972 *Paspalorum*), and *C. citrina* (sect. *Citrinae*). Colored hexbins indicate the intergenic lengths of
973 all genes with color-code indicating the frequency distribution (gene count) according to the
974 legend on the right. Overlaid markers indicate specific gene types corresponding to legends in
975 the top right within each plot. Line graphs (top and right of each plot) depict the frequency
976 distributions of specific gene types (corresponding legend color) and all other genes not of the
977 specific type (black). For visualization purposes the first genes of contigs (5' end) are plotted
978 along the x-axis and the last gene of each contig (3' end) are plotted along the y-axis. For
979 information on statistical test see Methods and for plots of all remaining isolates see Additional
980 file 1: Figure S10.
981
982 **Figure 6:** Representative isolates of each *Claviceps* species showing the fraction of BLAST hits
983 at a given % identity (y-axis) within each isolate (z-axis) at a given percent identity (x-axis) from
984 the second closet BLASTp match of proteins within each isolate's own genome. Two *C.*
985 *purpruea* s.s. isolates are shown to compare a newly sequenced genome versus the reference.
986

987 **Figure 7:** Heatmap of gene counts in orthogroups for all 53 *Claviceps* strains ordered based on
988 ML tree in Fig. 1 and separated by sections. Orthogroups are separated based on their
989 classification and are only represented once (i.e. secondary (2°) metabolite orthogroups shown
990 are those that are not already classified into the effector or secreted orthogroups) and are ordered
991 based on hierarchical clustering, see Additional file 2: Table S9 for list of orthogroups
992 corresponding to the order shown in the heatmaps. The host spectrum (right) is generalized
993 across species, as no literature has determined the existence of race specific isolates within
994 species, is shown on the left side of the figure determined from literature review of field
995 collected samples (Supplementary Material in Píchová *et al.* 2018) and previous inoculation tests
996 Campbell (1957) and Liu *et al.* (*Submitted*). For heatmap of conserved domains see Additional
997 file 1: Figure S12 and for unclassified gene families see Additional file 1: Figure S13.

Table 1: Assembly and annotations statistics for the three reference *Claviceps* genomes and the 50 *Claviceps* genomes used in this study.

Organism	Strain	Section	Host of Origin: Family / Tribe	Host of Origin: Genus / species	Read Coverage	Genome size (Mb)	Contig (#)	N50	Genomic GC (%)	TE§ content (%)	Gene count	BUSCO Completeness: Dikarya	BUSCO Completeness: Sordario-myceta
References:													
C. purpruea	20.1	Claviceps	Triticeae	*Secale cereale*	--	32.1	1,442†	46,498†	51.6%	10.9%	8,703	95.30%	94.70%
C. fusiformis	PRL1980	Pusillae	Paniceae	*Pennisetum typhoideum*	--	52.3	6,930	19,980	37.3%	47.5%	9,304	96.70%	94.90%
C. paspali	RRC1481	Paspalorum	Paspaleae	*Paspalum* sp.	--	28.9	2,304	26,898	47.7%	17.5%	8,400	94.30%	93.30%
This study:													
C. purpruea	Clav04	Claviceps	Bromeae	*Bromus inermis*	46x	31.8	3,288	21,051	51.7%	10.1%	8,824	95.50%	94.10%
C. purpruea	Clav26	Claviceps	Triticeae	*Hordeum vulgare*	59x	30.8	1,361	49,697	51.7%	9.1%	8,737	97.70%	96.50%
C. purpruea	Clav46	Claviceps	Triticeae	*Secale cereale*	58x	30.8	1,409	49,302	51.7%	9.7%	8,597	98.00%	96.60%
C. purpruea	Clav55	Claviceps	Poeae	*Lolium perenne*	59x	30.7	1,525	44,299	51.8%	9.8%	8,480	97.10%	95.90%
C. purpruea	LM4	Claviceps	Triticeae	*Tricosecale*	64x	30.6	1,296	47,441	51.8%	10.0%	8,470	97.00%	95.80%
C. purpruea	LM5	Claviceps	Triticeae	*Hordeum vulgare*	67x	30.5	1,258	51,505	51.8%	9.0%	8,508	96.90%	95.50%
C. purpruea	LM14	Claviceps	Triticeae	*Hordeum vulgare*	49x	30.6	1,297	49,955	51.8%	10.0%	8,422	97.40%	95.60%
C. purpruea	LM28	Claviceps	Triticeae	*Triticum aestivum*	49x	30.6	1,343	51,635	51.7%	9.6%	8,713	97.30%	96.10%
C. purpruea	LM30	Claviceps	Triticeae	*Secale cereale*	64x	30.6	1,224	51,374	51.8%	9.4%	8,526	97.00%	95.50%
C. purpruea	LM33	Claviceps	Triticeae	*Secale cereale*	45x	30.5	1,398	44,564	51.8%	9.2%	8,557	96.30%	95.50%
C. purpruea	LM39	Claviceps	Triticeae	*Triticum turgidum subsp. durum*	81x	30.5	1,282	48,443	51.8%	10.1%	8,591	97.10%	96.10%
C. purpruea	LM46	Claviceps	Triticeae	*Triticum turgidum subsp. durum*	79x	30.6	1,291	50,932	51.8%	9.6%	8,455	97.00%	95.80%
C. purpruea	LM60	Claviceps	Poeae	*Avena sativa*	81x	30.6	1,259	47,464	51.7%	9.3%	8,498	97.00%	95.80%
C. purpruea	LM71	Claviceps	Poeae	*Alopercurus myosuroides*	168x	30.5	1,400	45,114	51.8%	9.6%	8,472	97.10%	95.60%
C. purpruea	LM207	Claviceps	Triticeae	*Elymus repens*	53x	30.5	1,352	45,388	51.8%	9.2%	8,475	97.00%	95.70%
C. purpruea	LM223	Claviceps	Bromeae	*Bromus riparius*	74x	30.8	1,297	46,577	51.7%	10.5%	8,438	97.00%	95.70%
C. purpruea	LM232	Claviceps	Poeae	*Phalaris canariensis*	53x	30.7	1,348	49,571	51.7%	9.4%	8,512	96.60%	95.70%
C. purpruea	LM233	Claviceps	Poeae	*Phalaris canariensis*	49x	30.6	1,331	50,327	51.8%	9.9%	8,717	96.70%	95.90%
C. purpruea	LM461	Claviceps	Triticeae	*Elymus repens*	37x	30.5	1,440	44,216	51.8%	8.4%	8,656	96.60%	95.20%
C. purpruea	LM469	Claviceps	Triticeae	*Triticum aestivum*	75x	30.5	1,257	48,403	51.8%	10.0%	8,394	97.30%	96.00%
C. purpruea	LM470	Claviceps	Triticeae	*Elymus repens*	26x	30.5	1,797	32,579	51.8%	9.0%	8,591	96.50%	95.30%
C. purpruea	LM474	Claviceps	Triticeae	*Hordeum vulgare*	64x	30.6	1,354	47,245	51.8%	9.4%	8,500	96.80%	95.70%
C. purpruea	LM582	Claviceps	Triticeae	*Secale cereale*	89x	30.7	1,600	39,003	51.8%	9.6%	8,518	97.20%	95.40%
C. aff. purpruea	Clav52	Claviceps	Poeae	*Poa pratensis*	60x	29.6	1,334	48,893	51.8%	8.2%	8,316	96.80%	96.20%
C. quebecensis‡	Clav32	Claviceps	Triticeae	*Hordeum vulgare*	64x	28.7	1,068	58,118	51.6%	4.5%	8,232	98.00%	96.60%
C. quebecensis‡	Clav50	Claviceps	Triticeae	*Elymus sp.*	59x	28.8	1,075	66,795	51.6%	6.9%	8,046	97.50%	96.30%
C. quebecensis‡	LM458	Claviceps	Poeae	*Ammophila* (plant)	78x	28.4	1,166	45,693	51.6%	6.1%	8,055	97.10%	95.80%
C. occidentalis‡	LM77	Claviceps	Poeae	*Phleum pratense*	58x	28.7	1,728	29,222	51.4%	6.0%	8,162	96.10%	94.70%
C. occidentalis‡	LM78	Claviceps	Bromeae	*Bromus inermis*	64x	28.8	1,689	29,608	51.4%	6.0%	8,231	95.80%	94.70%
C. occidentalis‡	LM84	Claviceps	Bromeae	*Bromus inermis*	164x	28.9	1,404	36,685	51.4%	6.0%	8,221	97.00%	95.40%
C. ripicola‡	LM218	Claviceps	Poeae	*Phalaris arundinacea*	146x	31.1	1,072	60,464	51.4%	10.3%	8,327	96.70%	95.70%
C. ripicola‡	LM219	Claviceps	Poeae	*Phalaris arundinacea*	55x	30.8	1,239	55,312	51.4%	9.5%	8,381	96.80%	95.80%
C. ripicola‡	LM220	Claviceps	Poeae	*Phalaris arundinacea*	91x	30.9	1,223	54,100	51.4%	9.3%	8,449	97.10%	95.90%
C. ripicola‡	LM454	Claviceps	Poeae	*Ammophila breviligulata*	156x	31.2	1,508	40,844	51.4%	8.4%	8,562	97.10%	96.10%
C. spartinae	CCC535	Claviceps	Zoysieae	*Sporobolus anglicus*	60x	29.3	1,456	42,688	51.4%	7.1%	8,433	97.50%	95.90%
C. arundinis	LM583	Claviceps	Molinieae	*Phragmites australis*	69x	30.6	996	70,672	51.4%	9.8%	8,235	96.80%	95.70%
C. arundinis	CCC1102	Claviceps	Molinieae	*Phragmites australis*	61x	30.3	896	91,905	51.4%	8.3%	8,486	97.70%	96.50%
C. humidiphila	LM576	Claviceps	Poeae	*Dactylis sp.*	77x	31.2	1,236	55,717	51.5%	9.9%	8,440	97.00%	95.90%
C. perihumidiphila‡	LM81	Claviceps	Triticeae	*Elymus albicans*	140x	31.2	1,003	67,487	51.5%	11.0%	8,291	97.10%	95.90%
C. cyperi	CCC1219	Claviceps	Cyperaceae (family)	*Cyperus esculentus*	56x	26.6	1,921	27,113	51.7%	8.9%	7,673	97.70%	95.40%
C. capensis	CCC1504	Claviceps	Ehrharteae	*Ehrharta villosa*	66x	27.7	1,136	59,777	51.7%	6.2%	8,037	97.60%	95.70%
C. pazoutovae	CCC1485	Claviceps	Stipeae	*Stipa dregeana*	61x	27.6	1,304	42,785	51.7%	6.8%	7,941	97.50%	96.00%
C. monticola	CCC1483	Claviceps	Brachypodieae	*Brachypodium sp.*	58x	27.8	1,144	56,619	51.6%	7.0%	7,977	98.10%	96.50%
C. pusilla	CCC602	Pusillae	Andropogoneae	*Bothriochloa insculpta*	52x	45.9	5,068	15,010	40.4%	42.1%	8,735	90.90%	88.30%
C. lovelessii	CCC647	Pusillae	Eragostidinae	*Eragrostis sp.*	53x	41.1	5,300	12,480	42.1%	33.9%	8,862	91.60%	88.20%
C. digitariae	CCC659	Pusillae	Paniceae	*Digitaria eriantha*	57x	33.4	1,773	32,638	44.8%	20.0%	8,285	95.90%	94.70%
C. maximensis	CCC398	Pusillae	Paniceae	*Megathyrsus maximus*	58x	33.0	829	81,956	44.9%	19.8%	7,943	98.30%	96.50%
C. sorghi	CCC632	Pusillae	Andropogoneae	*Sorghum bicolor*	60x	35.6	3,660	16,225	44.4%	30.4%	8,208	89.90%	87.10%
C. africana	CCC489	Pusillae	Andropogoneae	*Sorghum bicolor*	56x	37.7	1,781	37,639	42.5%	34.0%	8,119	95.00%	91.50%
C. citrina	CCC265	Citrinae	Cynodonteae	*Distichlis spicata*	64x	43.5	4,772	16,294	41.5%	51.7%	7,821	92.20%	88.20%

† The reference strain *C. purpurea* 20.1 was additionally assembled into 191 scaffolds with a scaffold N50 of 433,221.
‡ Newly identified species Liu *et al.* (*Submitted*)
§ Transposable element (TE) content represented as percent of the genome masked by TEs

Fig. 1

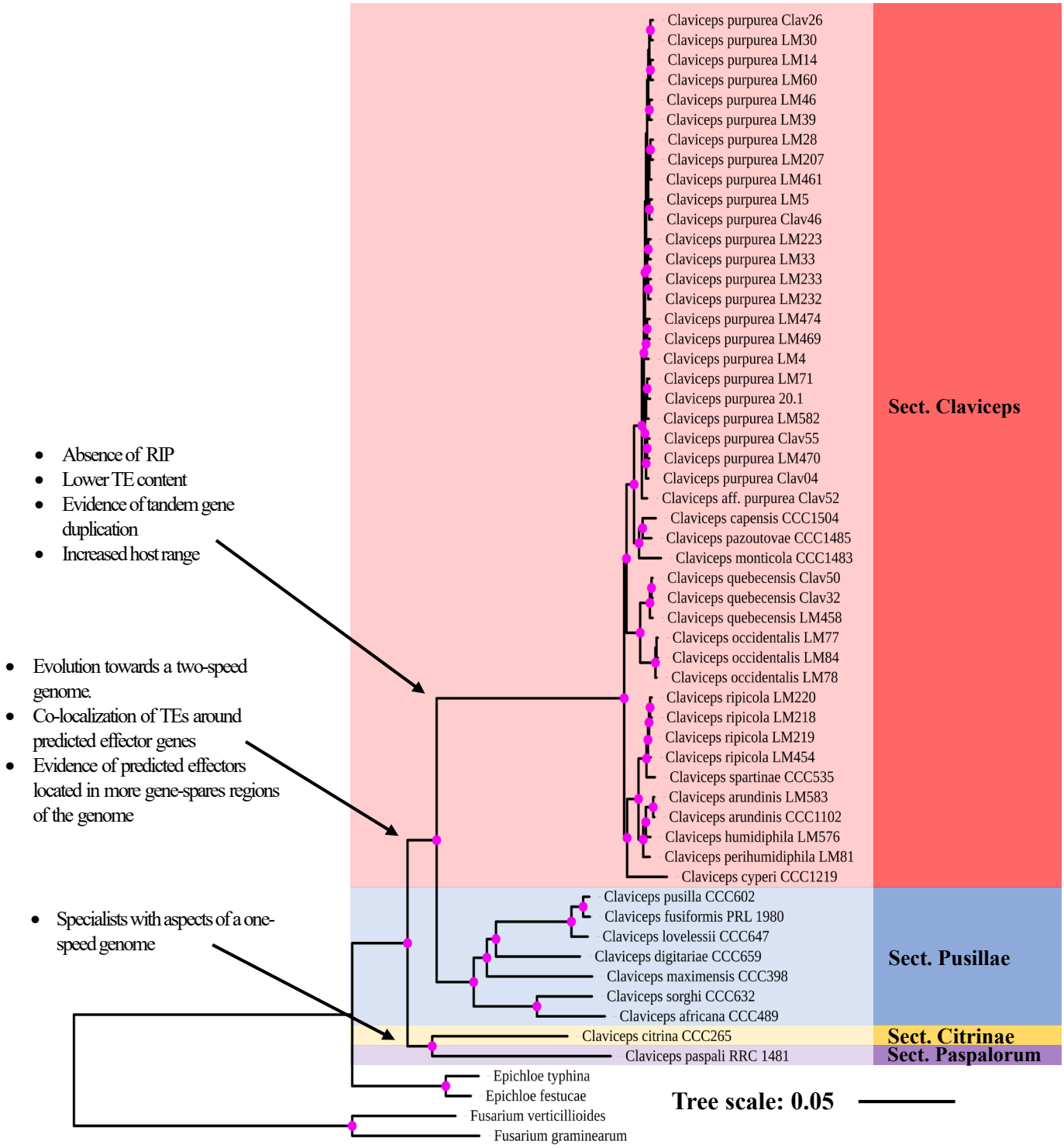
Claviceps purpurea Clav26
Claviceps purpurea LM30
Claviceps purpurea LM14
Claviceps purpurea LM60
Claviceps purpurea LM46
Claviceps purpurea LM39
Claviceps purpurea LM28
Claviceps purpurea LM207
Claviceps purpurea LM461
Claviceps purpurea LM5
Claviceps purpurea Clav46
Claviceps purpurea LM223
Claviceps purpurea LM33
Claviceps purpurea LM233
Claviceps purpurea LM232
Claviceps purpurea LM474
Claviceps purpurea LM469
Claviceps purpurea LM4
Claviceps purpurea LM71
Claviceps purpurea 20.1
Claviceps purpurea LM582
Claviceps purpurea Clav55
Claviceps purpurea LM470
Claviceps purpurea Clav04
Claviceps aff. purpurea Clav52
Claviceps capensis CCC1504
Claviceps pazoutovae CCC1485
Claviceps monticola CCC1483
Claviceps quebecensis Clav50
Claviceps quebecensis Clav32
Claviceps quebecensis LM458
Claviceps occidentalis LM77
Claviceps occidentalis LM84
Claviceps occidentalis LM78
Claviceps ripicola LM220
Claviceps ripicola LM218
Claviceps ripicola LM219
Claviceps ripicola LM454
Claviceps spartinae CCC535
Claviceps arundinis LM583
Claviceps arundinis CCC1102
Claviceps humidiphila LM576
Claviceps perihumidiphila LM81
Claviceps cyperi CCC1219
Claviceps pusilla CCC602
Claviceps fusiformis PRL 1980
Claviceps lovelessii CCC647
Claviceps digitariae CCC659
Claviceps maximensis CCC398
Claviceps sorghi CCC632
Claviceps africana CCC489
Claviceps citrina CCC265
Claviceps paspali RRC 1481
Epichloe typhina
Epichloe festucae
Fusarium verticillioides
Fusarium graminearum
Sect. Claviceps
Sect. Pusillae
Sect. Citrinae
Sect. Paspalorum
Tree scale: 0.05
Absence of RIP
Lower TE content
Evidence of tandem gene duplication
Increased host range
Evolution towards a two-speed genome.
Co-localization of TEs around predicted effector genes
Evidence of predicted effectors located in more gene-spares regions of the genome
Specialists with aspects of a one-speed genome

Fig. 2

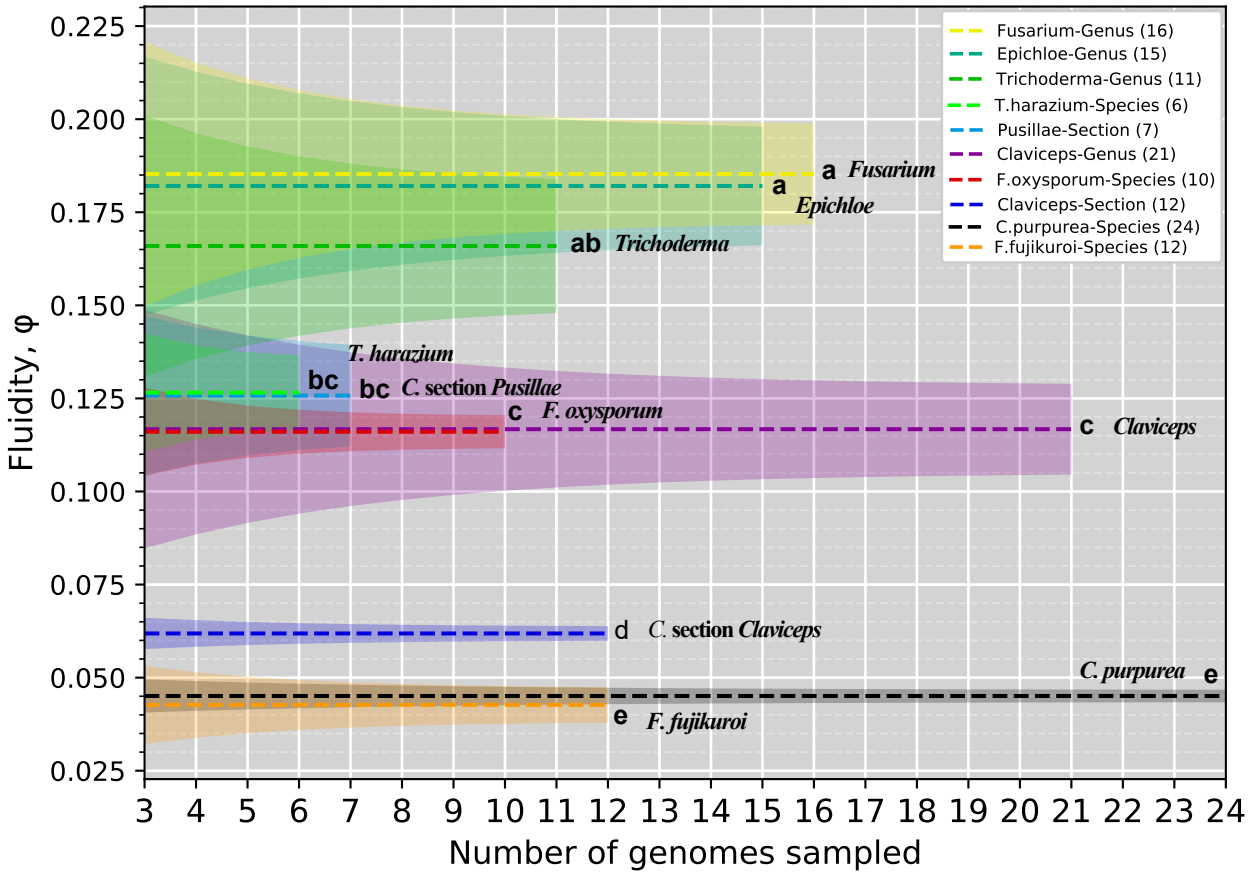
Fusarium-Genus (16)
Epichloe-Genus (15)
Trichoderma-Genus (11)
T.harazium-Species (6)
Pusillae-Section (7)
Claviceps-Genus (21)
F.oxysporum-Species (10)
Claviceps-Section (12)
C.purpurea-Species (24)
F.fujikuroi-Species (12)
a Fusarium
a Epichloe
ab Trichoderma
T. harazium
bc
bc C. section Pusillae
c F. oxysporum
c Claviceps
d C. section Claviceps
C. purpurea e
e F. fujikuroi
Fluidity, φ
0.225
0.200
0.175
0.150
0.125
0.100
0.075
0.050
0.025
3 4 5 6 7 8 9 10 11 12 13 14 15 16 17 18 19 20 21 22 23 24
Number of genomes sampled

Fig. 3

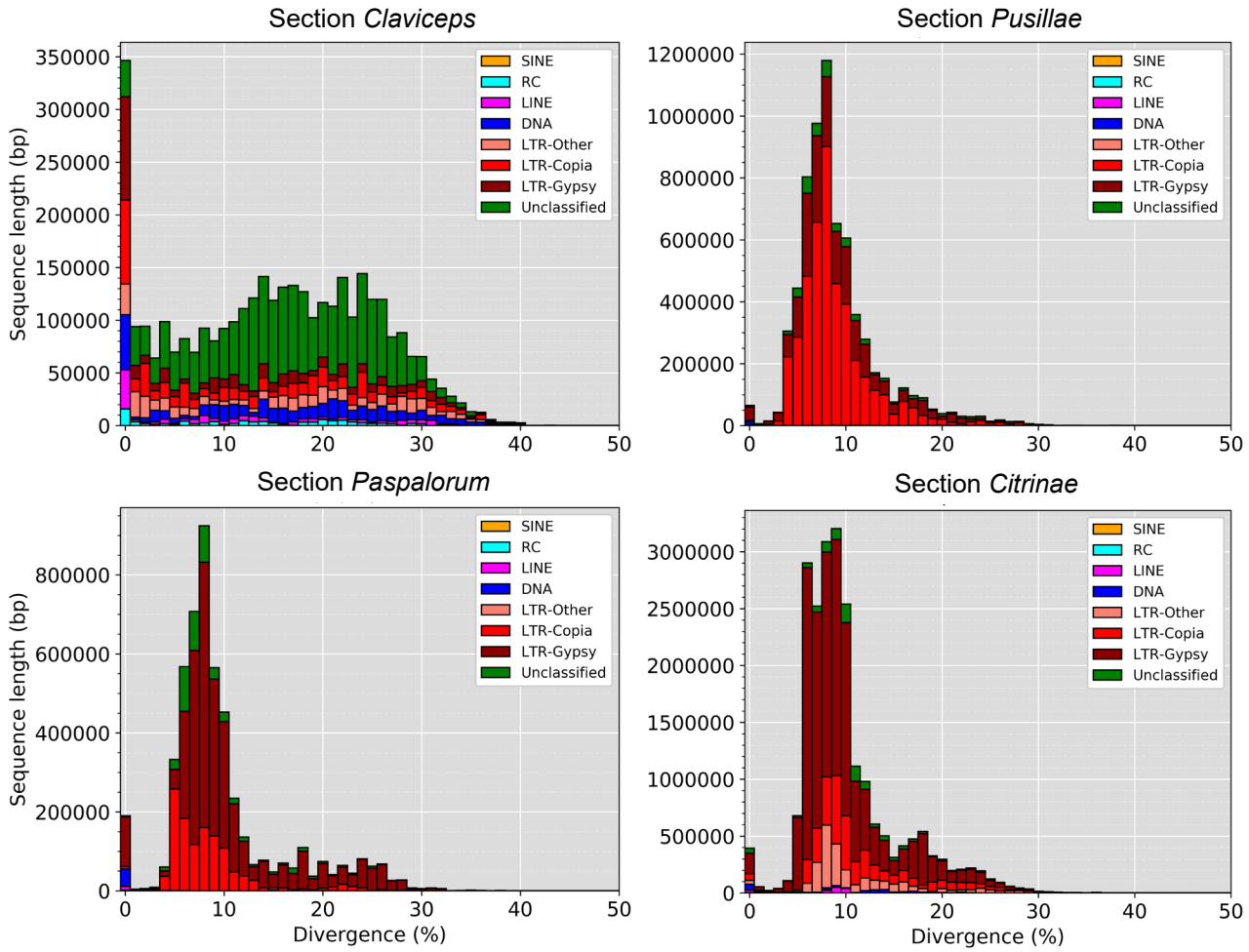
Section *Claviceps*
Section *Pusillae*
Section *Paspalorum*
Section *Citrinae*
Sequence length (bp)
Divergence (%)
SINE
RC
LINE
DNA
LTR-Other
LTR-Copia
LTR-Gypsy
Unclassified

Fig. 4

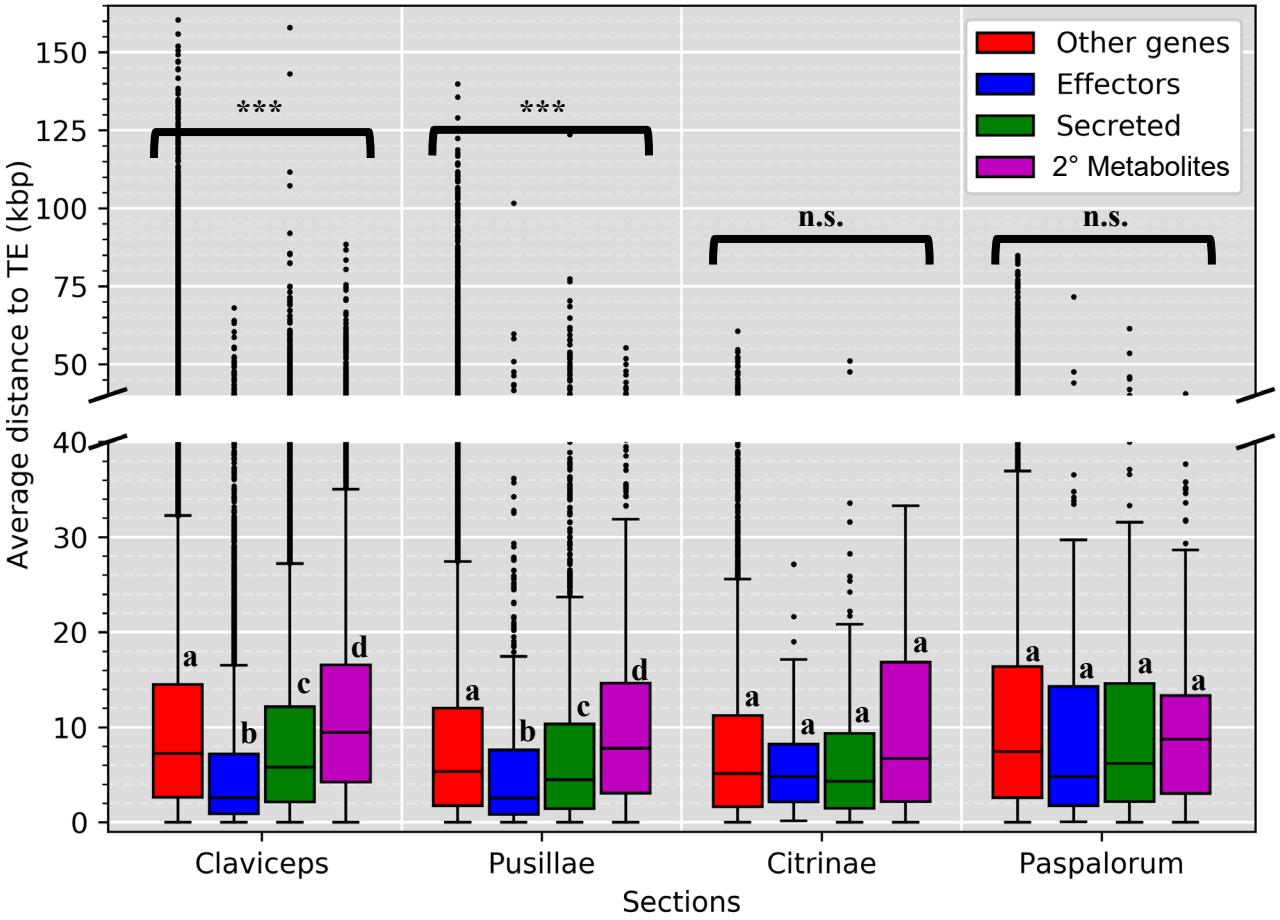
Other genes
Effectors
Secreted
2° Metabolites
***
***
n.s.
n.s.
Average distance to TE (kbp)
150
125
100
75
50
40
30
20
10
0
a
b
c
d
a
b
c
d
a
a
a
a
a
a
a
a
Claviceps
Pusillae
Citrinae
Paspalorum
Sections

Fig. 5

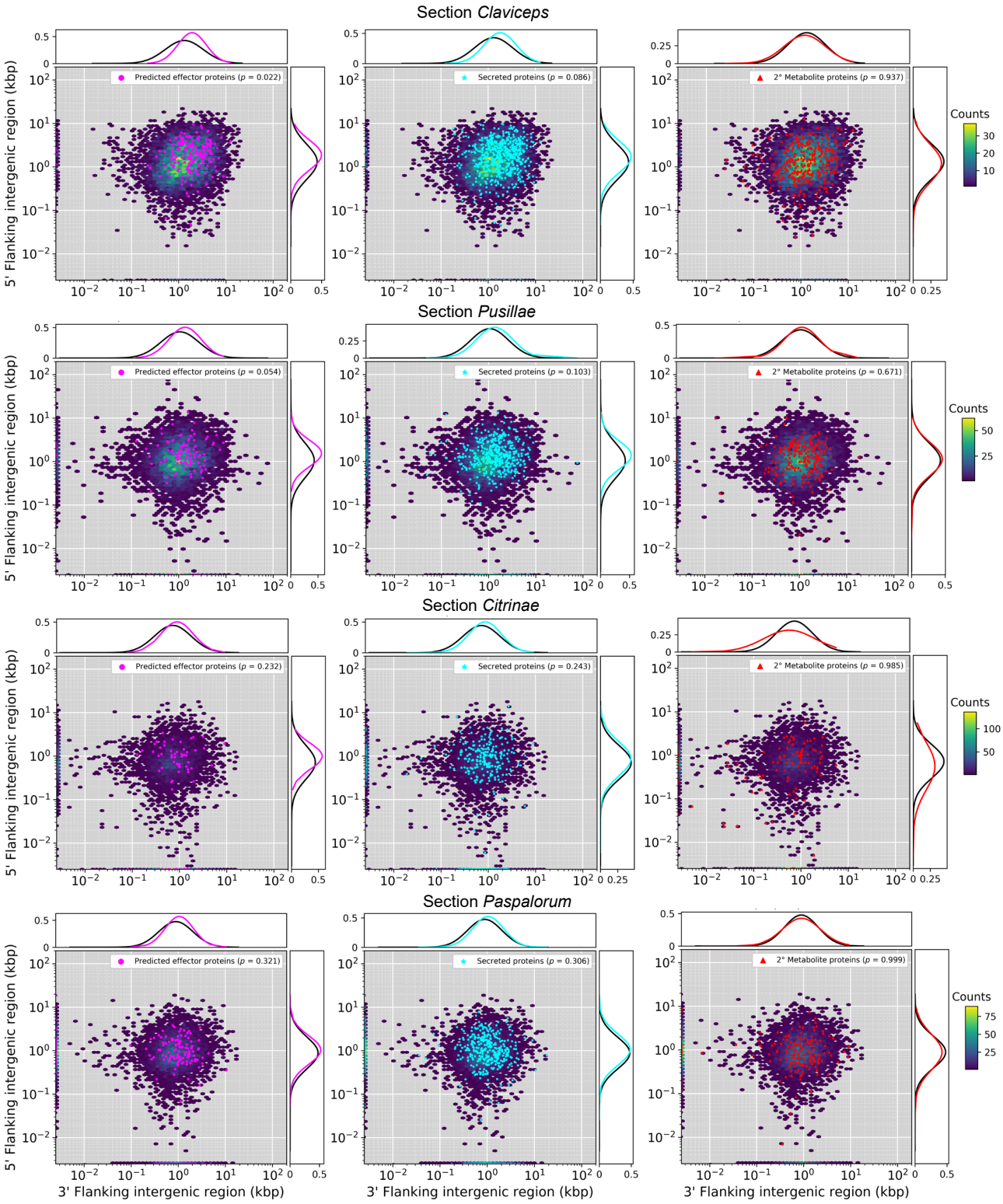
Section Claviceps
Predicted effector proteins (p = 0.022)
Secreted proteins (p = 0.086)
2° Metabolite proteins (p = 0.937)
Section Pusillae
Predicted effector proteins (p = 0.054)
Secreted proteins (p = 0.103)
2° Metabolite proteins (p = 0.671)
Section Citrinae
Predicted effector proteins (p = 0.232)
Secreted proteins (p = 0.243)
2° Metabolite proteins (p = 0.985)
Section Paspalorum
Predicted effector proteins (p = 0.321)
Secreted proteins (p = 0.306)
2° Metabolite proteins (p = 0.999)
Counts
5' Flanking intergenic region (kbp)
3' Flanking intergenic region (kbp)

Fig. 6

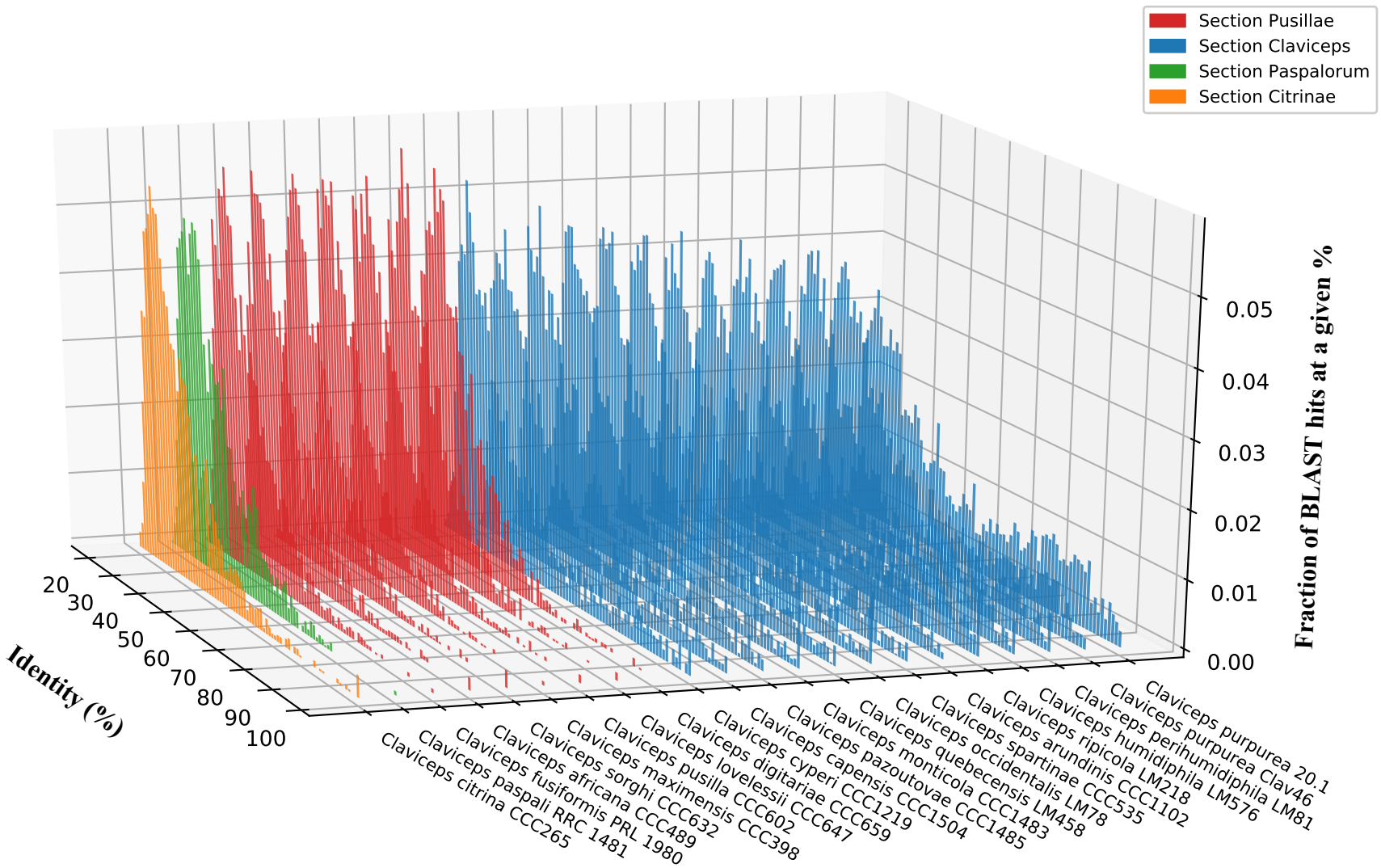
Section Pusillae
Section Claviceps
Section Paspalorum
Section Citrinae
Fraction of BLAST hits at a given %
0.00
0.01
0.02
0.03
0.04
0.05
Identity (%)
20
30
40
50
60
70
80
90
100
Claviceps purpurea 20.1
Claviceps purpurea Clav46
Claviceps perihumidiphila LM576
Claviceps humidiphila LM81
Claviceps ripicola LM218
Claviceps arundinis CCC1102
Claviceps spartinae CCC535
Claviceps occidentalis LM78
Claviceps quebecensis LM458
Claviceps monticola CCC1483
Claviceps pazoutovae CCC1504
Claviceps capensis CCC1485
Claviceps cyperi CCC1219
Claviceps digitariae CCC659
Claviceps lovelessii CCC647
Claviceps pusilla CCC602
Claviceps maximensis CCC398
Claviceps sorghi CCC632
Claviceps africana CCC489
Claviceps fusiformis PRL 1980
Claviceps paspali RRC 1481
Claviceps citrina CCC265

Fig. 7

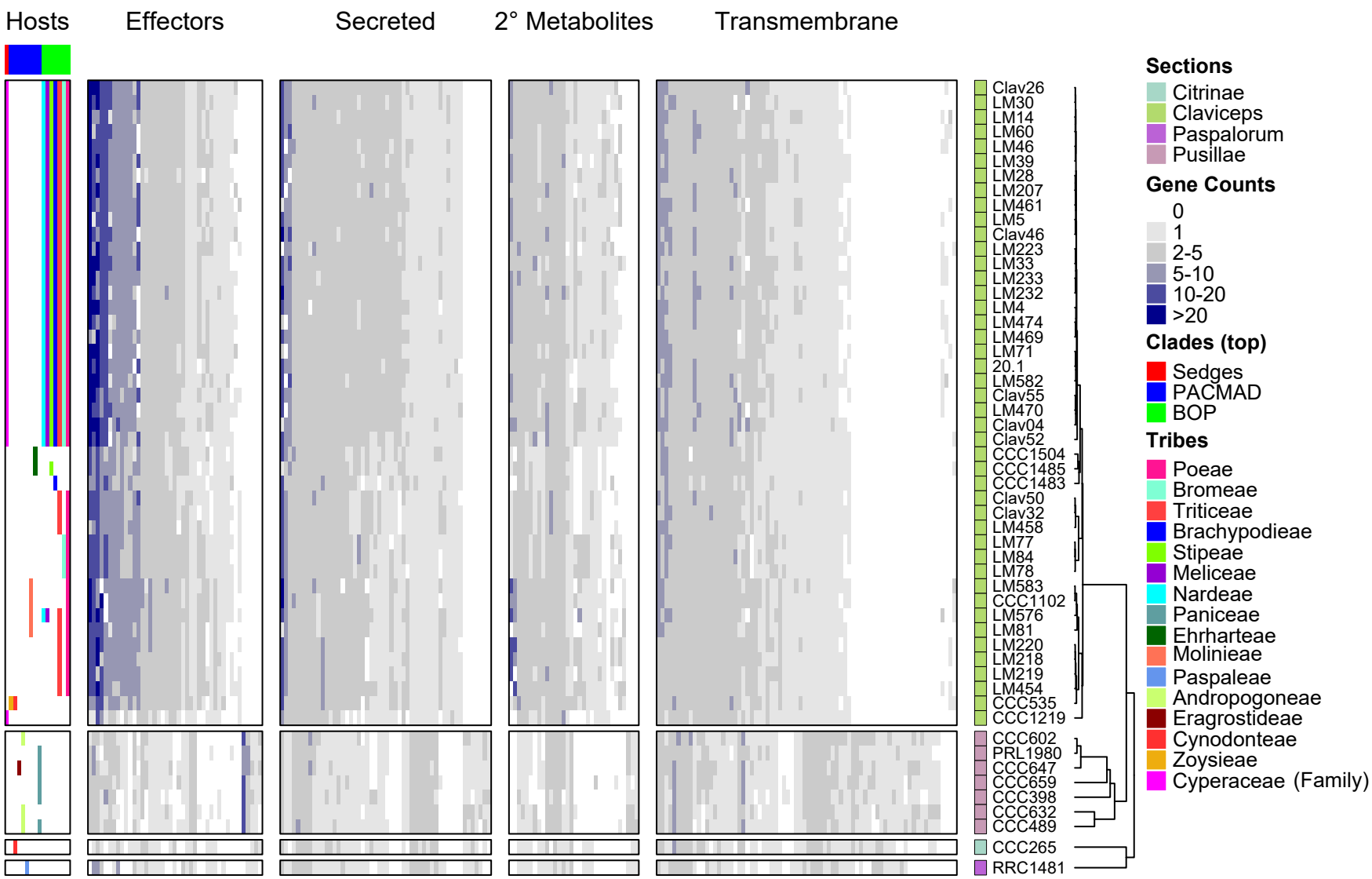
Hosts
Effectors
Secreted
2° Metabolites
Transmembrane
Clav26
LM30
LM14
LM60
LM46
LM39
LM28
LM207
LM461
LM5
Clav46
LM223
LM33
LM233
LM232
LM4
LM474
LM469
LM71
20.1
LM582
Clav55
LM470
Clav04
Clav52
CCC1504
CCC1485
CCC1483
Clav50
Clav32
LM458
LM77
LM84
LM78
LM583
CCC1102
LM576
LM81
LM220
LM218
LM219
LM454
CCC535
CCC1219
CCC602
PRL1980
CCC647
CCC659
CCC398
CCC632
CCC489
CCC265
RRC1481
Sections
Citrinae
Claviceps
Paspalorum
Pusillae
Gene Counts
0
1
2-5
5-10
10-20
>20
Clades (top)
Sedges
PACMAD
BOP
Tribes
Poeae
Bromeae
Triticeae
Brachypodieae
Stipeae
Meliceae
Nardeae
Paniceae
Ehrharteae
Molinieae
Paspaleae
Andropogoneae
Eragrostideae
Cynodonteae
Zoysieae
Cyperaceae (Family)